Hybridization of Energy Storage Systems for Grid Support by Means of Bidirectional Power Electronic Converters

by

Ramy Georgious Zaher Georgious

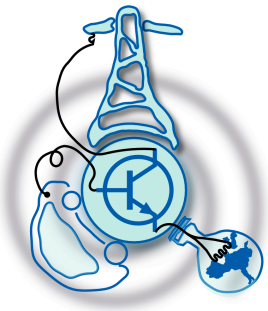

Submitted to the Department of Electrical Engineering, Electronics, Computers and Systems
in partial fulfillment of the requirements for the degree of
Master of Science in Electrical Energy Conversion and Power Systems
at the
UNIVERSIDAD DE OVIEDO
June 2014

Author .....
Ramy Georgious Zaher Georgious

Certified by .....
Jorge García García
Associate Professor
Thesis Supervisor

Hybridization of Energy Storage Systems for Grid Support by Means of Bidirectional Power Electronic Converters

by

Ramy Georgious Zaher Georgious

Submitted to the Department of Electrical Engineering, Electronics, Computers and Systems
on June 19, 2014, in partial fulfillment of the
requirements for the degree of
Master of Science in Electrical Energy Conversion and Power Systems

Abstract

This thesis deals with the simulation and real-time emulation in a laboratory setup of a Hybrid Energy Storage System connected to microgirds. The association of two batteries; i.g., Vanadium Redox Flow Battery and Lithium Ion battery permits to take advantage of the characteristics of both Energy Storage Systems obtaining a high energy density, high power density. A general model of Vanadium Redox Flow Battery is developed. A Vanadium Redox Flow battery and Lithium-Ion battery are connected to DC bus and controllable loads through two bidirectional boost converter. The model of the Vanadium Redox Flow battery is implemented in MATLAB/SIMULINK ®. The real-time experimental emulation of the Energy Storage System models and Hybrid Energy Storage System have been validated against PC simulations showing full consistency. The setup of the hardware can be used to test any technologies of batteries.

Thesis Supervisor: Jorge García García
Title: Associate Professor

Acknowledgments

I would like to thank my Master Thesis supervisor Prof. Jorge García García for his guidance and supporting during the Master and especially during the Master Thesis. I would Like to thank Prof. Pablo García Fernández for his help.

I would like to thank my parents as they taught me how to work hard and never give up. Many thanks to my mother for her support, encourage and her prayers for me.

I dedicate my Thesis to the soul of my father.

Agradecimientos

Qiuero agradecer a mi director de Trabajo Fin de Master, el profesor Jorge García García, por su guía y su apoyo durante el Máster, specialmente durante la realización del presente Trabajo. También quiero expresar mi agradecimiento al profesor Pablo García Fernández por su ayuda.

Quiero agradecer a mis padres, que me enseñarion a trabajar duro y a no rendirme nunca. Muchas gracias a mi madre, por su apoyo, por su constante aliento y por sus oraciones.

Dedico este Trabajo finde Máster a la memoria de mi Padre.

Contents

List of Figures

List of Tables

Chapter 1

Introduction

The main purpose of Energy Storage Systems (ESS) introduction in microgrids is to increase power quality, by maintaining power and energy balance in case any contingency is presented in the grid. The nature of these contingencies (ranging from load fluctuations even to islanding mode) will define the size of the ESS. Unfortunately none of the currently available ESS has the necessary high power and energy densities in the same time to face the effect of different disturbances coming from the load. An ESS must have a high power density in order to face fast power variations, and at the same time it must have a high energy density to give autonomy to the microgrids. Thus, the association of more than one storage technology in a Hybrid Energy Storage System (HESS) can be used to satisfy the above mentioned requirements. The HESS is usually formed by two complementary storage devices, one of high energy density and the other of high power density [1], [2], [3], [4], [5], [6].

1.1 Technologies of Energy Storage Systems

Nowadays, There are a lot of ESS technologies which are divided to short term (seconds), medium term (minutes) and long term (hours), ESS can be used within stand-alone applications [7], [8], [9], [10].

1. Mechanical Storage System:

   (a) Flywheel Storage System.

   (b) Compressed Air Storage System.

   (c) Pumped Hydroelectric Storage System.

2. Electrochemical Storage System:

   (a) Conventional Batteries.

   (b) Flow Batteries.

3. Electromagnetic Storage System:

   (a) Superconducting Magnetic Energy Storage System.

4. Electrical Storage System:

   (a) Conventional capacitors.

   (b) Supercapacitors.

1.2 Comparison of the Batteries over Other Types of Energy Storage Systems

The main advantages and drawbacks of Electrochemical Storage System versus other ESS technologies are summarized in Table 1.1.

Table 1.1: Advantages and Drawbacks of Electrochemical Storage System (Batteries)

Advantages of the batteries [7]	Drawbacks of the batteries [7]
A high flexibility in terms of size.	Efficiency dependent on electrochemistry.
Quick response .	A high capital cost.
Up to hours of continuous operations.	

1.2.1 Technologies of Batteries

1. Conventional batteries:
   (a) Lithium-Ion battery (LI-IB).
   (b) Lead-Acid battery.
   (c) Nickel-Cadmium battery.
   (d) Nickel Metal Hydride battery.
   (e) Sodium-Sulfur battery.
   (f) Nickel-Hydrogen battery.
2. Flow batteries:
   (a) Vanadium Redox Flow Battery (VRFB).
   (b) Zinc-Bromine Flow Battery.

1.3 Selection of the Batteries

The system have two different batteries with different dynamics. Vanadium Redox Flow Battery (VRFB) is used for supplying the load as it has high energy density while the Lithium-Ion battery (LI-IB) is used for supplying the load at the transient with the Vanadium Redox Flow Battery (VRFB) as it has high power density. The advantages of VRFB [2], [11], [12], [13], [14], [15], [16] and Li-ion [7], [9] are in Table 1.2.

The life cycle of the VRFB is up to 10 000 charge / discharge cycles and it lasts for minutes or hours, on the other hand, the life cycle of the LI-IB is 3000 charge / discharge cycles and it lasts for seconds to minutes [13].

The interconnection of the HESS with the microgrid can be done in different ways, but the most common solution is to use two separate DC/DC Convertors in order to control the ESS individually [1], [6], [13]. With this topology, the power flow of each storage device can be controlled independently thanks to the two DC/DC Converters,

Table 1.2: Advantages of VRFB and LI-IB

VRFB	LI-IB
Energy storage device. It is intended for energy rather than for power.	Power storage device.
Their high storage efficiency. It can work for hours.	Quick response compared to VRFB.
High scalability. It is suitable for Large scale storage applications because of electrolyte tanks.	Operation through a wide range of temperatures and it has high efficiency.
Instant recharge by electrolyte exchange.	Easy charge controllability and low self-discharge.
Long life cycle up to 10 000 charge/discharge cycles leads to lower through life costs.	Suitable for short term applications.
Low maintenance requirements because it uses pumps to circulate the electrolytes from the tanks to the cell.	No pollution.

offering a high flexibility to manage the HESS. The biggest disadvantage of this topology is the increased number of components and consequently their associated losses.

The system is formed by two batteries with different dynamics, that are connected connected to the DC bus through two bidirectional boost converter and two controllable loads connected in parallel with the DC bus as shown in Figure 1-1. However, the VRFB is not cost effective in high power applications. The use of Li-IB which has a high power density in parallel with the VRFB can reduce its power rating and, therefore, the cost also [2],[3].

1.4 Outline

In Chapter 1, The technologies of energy storage systems and especially batteries , will be described. Also, the reasons of selections the VRFB and Li-IB for the hybrid system will be explained.

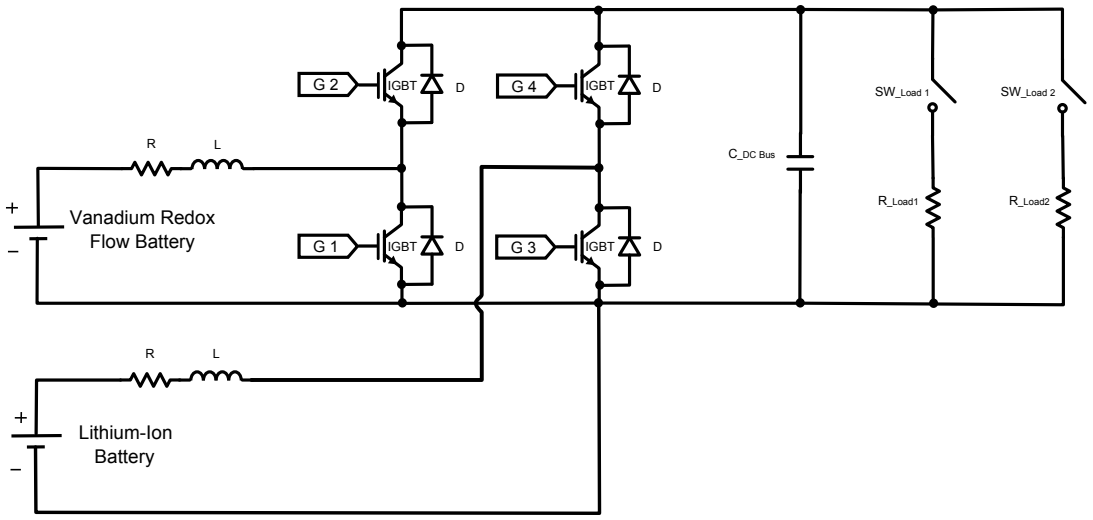

Figure 1-1: The power circuit of the system.

In Chapter 2, A general modeling of a generic ESS, particularized for the above-mentioned technologies, for all ranges of power and energy is developed and implemented in MATLAB/SIMULINK ®.

In Chapter 3, It will be shown the emulating procedure for VRFB and Li-IB, including a software emulation of their dynamic behavior.

In Chapter 4, The control strategy for the power converters (boost converters) of both ESS are presented. The control of the first boost converter is controlling the DC bus voltage. The control of the second boost converter is controlling the peak transient power when load varies suddenly.

In Chapter 5, Simulation results obtained from using MATLAB/SIMULINK ® and experiments results from implementation are presented.

Conclusions and future developments will be presented in final Chapter 6.

Chapter 2

Modeling of the Batteries

2.1 Introduction

A general model of VRFB will be developed which will depend on physical and mathematical properties of the battery [1], [2], [3], [8], [11], [12],[13], [14], [17], [18], [19], [20], [21]. This model can be used for any range of power and energy rating including the losses. A general model of LI-IB will be used from MATLAB/SIMULINK®.

2.2 Vanadium Redox Flow Battery

A VRFB is an electrochemical cell divided into two compartments by an ionic membrane where the battery reaction takes place, the positive and negative vanadium electrolytes are stored in two tanks as shown in figure 2-1. The electrolytes are pumped from the tanks to the cell for circulating through a pump in each compartment to improve battery performance and efficiency [8], [15], [22], [23].

The active material used for both the positive and negative electrodes of the VRFB is vanadium ions that are dissolved in sulfuric acid and serve as metal ions whose valence number changes.

VRFB uses a controlled pump to induce flow, and improve battery performance and efficiency. The state of Charge (SOC) represents the amount of active chemicals in the system.

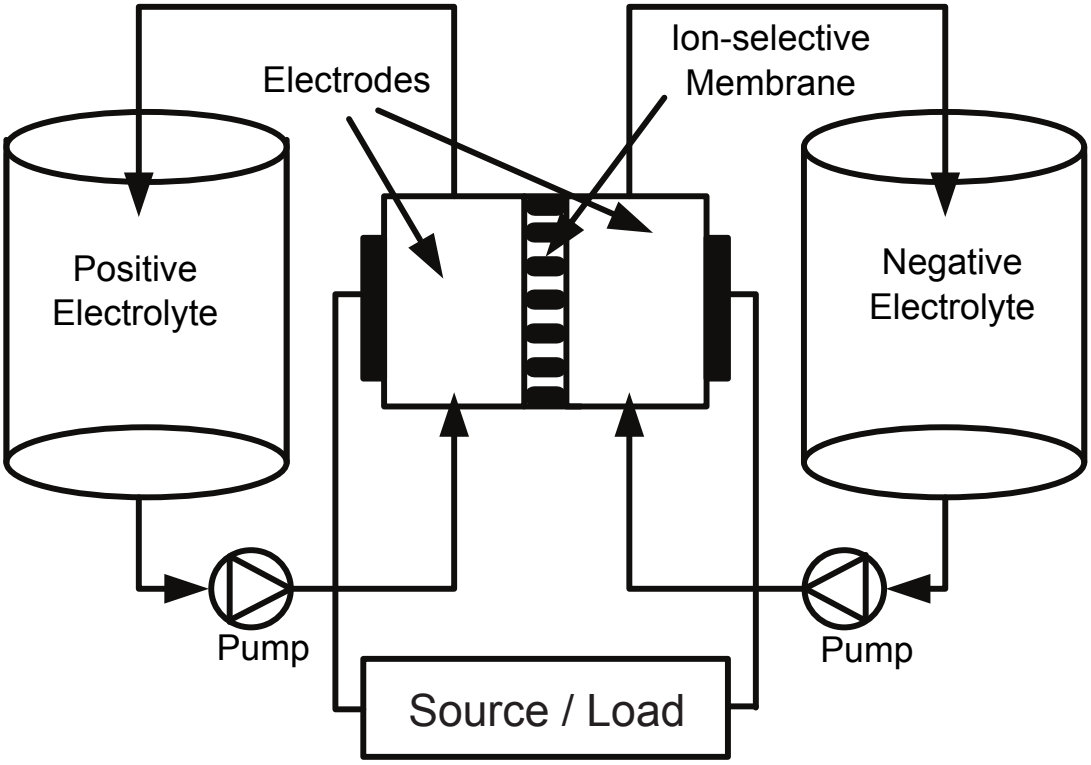

Figure 2-1: VRFB operating principle
[8],[15],[24].

The power and voltage ratings of a VRFB depends on the cell stack, while the energy capacity depends on the tank size and volume of electrolyte. This independence between energy and power ratings provides high flexibility in terms of design.

In practice, the operation is limited to a SOC between 20 % and 80%, due to over voltage issues on charging and under voltage issues on discharging.

The operating point where the stack current is maximum, 20 % SOC and the overall efficiency is supposed to be 79 %. The calculations are based on estimating losses at the end of the discharge cycle of 20 % SOC.

The total operating losses are divided into internal losses and parasitic losses. The internal losses are divided into reaction losses and resistive losses. The parasitic losses are divided into fixed losses and variable losses. The percentage of the losses of VRFB are shown in Table 2.1.

Table 2.1: Losses in the VRFB

Losses	Percentage %
Total operating losses	21
Internal losses	15
Reaction losses	9
Resistive losses	6
Parasitic losses	6
Fixed losses	2
variable losses	4

2.3 Properties of the Model

This model is based on researchers papers [1], [2], [3], [8], [11], [12], [13], [14], [17], [18], [19], [20], [21].

1. The stack voltage is modeled as a controlled voltage source.

2. The parasitic losses accounts for power consumption by the re-circulation pump, the system controller and power loss from cell stack by-pass currents.

(a) The fixed losses due to system controller and stack by-pass currents is modeled as a fixed resistance .

(b) The variable pump losses due to the re-circulation pump are modeled as a controlled current source.

3. The internal losses accounts for the losses due to reaction kinetics, mass transport resistance, solution resistance, electrode resistance and bipolar plate resistance.

   (a) The Reaction losses due to reaction kinetics are modeled as a reaction resistance.

   (b) The resistive losses due to mass transport resistance, solution resistance, electrode resistance and bipolar plate resistance are modeled as a resistive losses resistance .

4. The SOC is modeled as a variable that is dynamically updated which represents the amount of active chemicals in the system.

5. The transient component associated with the electrode is modeled as a capacitance.

2.4 Modeling

The equivalent circuit of VRFB is shown in Figure 2-2. The parameters of the equivalent circuit are calculating as following:

2.4.1 Output Terminal Voltage Estimation

The battery individual cell voltage is directly related to the SOC of the battery based on the Nernst equation [7] is:

$$V_{cell} = V_{equilibrium} + 2 * \frac{R * T}{F} * Ln\left(\frac{SOC}{1 - SOC}\right) \tag{2.1}$$

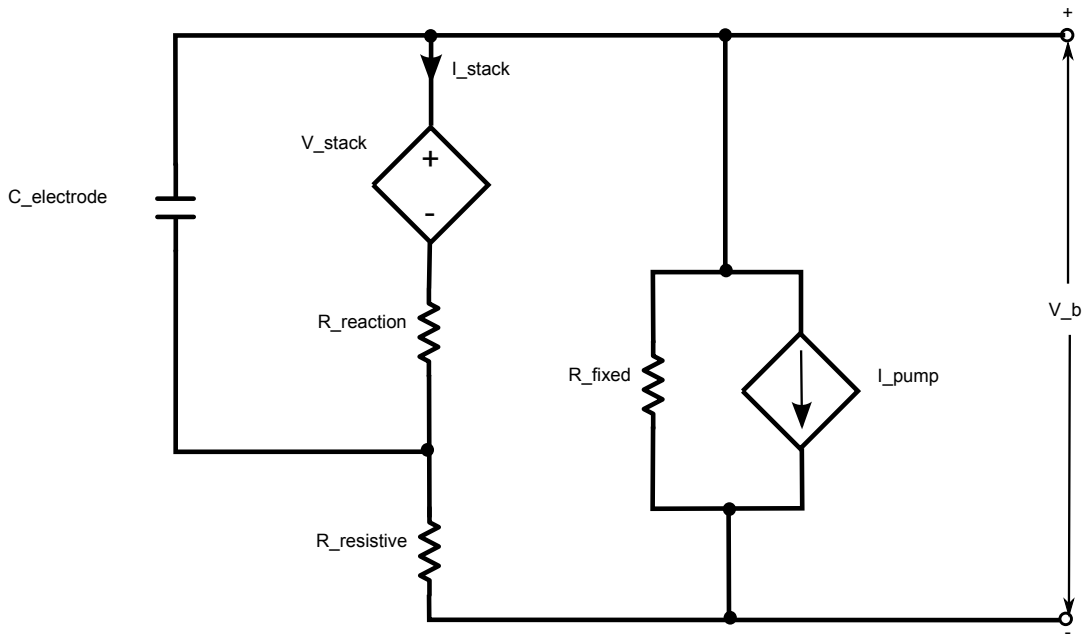

Figure 2-2: The equivalent circuit of VRFB.

Where:

- $V_{equilibrium}$: is the standard cell potential at a SOC of 50 % equals to 1.25 V [25], [26].
- R: is the universal gas constant equals to 8.31451 J/(K.mole).
- T: is the temperature impact on the battery operation.
- F: is the Faraday constant equals to 96485 C/mol.
- SOC : is the State of Charge.

The single cell voltage is low, so the VRFB is made up of a number of cells in series. For a battery made of n cell stack, The battery internal stack voltage depends on the SOC and the number of cell stacks. The internal stack voltage or open circuit battery voltage can be expressed as following:

$$V_{Stack} = n * V_{cell} \tag{2.2}$$

$$= n * \left(V_{equilibrium} + 2 * \frac{R * T}{F} * Ln \left(\frac{SOC}{1 - SOC} \right) \right) \tag{2.3}$$

Where:

- n : is the number of cell stacks.

The battery output terminal voltage can be espressed as following:

$$V_b = V_{Stack} - I_{Stack} * (R_{reaction} + R_{resistive}) \tag{2.4}$$

Where:

- I_{Stack} : is the current flowing through the stack and it is positive during charge, negative during discharge.
- $R_{reaction}$: is the reaction resistance.
- $R_{resistive}$: is the resistive resistance.

2.4.2 Resistive Losses and Reaction Resistances Calculation

The total losses is 21 % as in Table 2.1 at maximum stack current and 20 % SOC. Then, the cell stack output power can be expressed as:

$$P_{stack} = \frac{P_{rating}}{1 - 0.21} \tag{2.5}$$

Where:

- P_{rating} : is the battery rated power.

The internal losses are divided into 9 % reaction losses and 6 % resistive losses, so the reaction and resistive resistance can be expressed as following:

$$R_{reaction} = \frac{0.09 * P_{stack}}{I_{max}^2} \tag{2.6}$$

$$R_{resisitive} = \frac{0.06 * P_{stack}}{I_{max}^2} \tag{2.7}$$

Where:

- I_{max} : is the maximum battery current.

2.4.3 Fixed Resistance and Pump Current Calculation

The parasitic losses are divided into 2 % fixed losses and 4 % variable losses, so the fixed and variable losses can be expressed as following:

$$P_{fixed} = 0.02 * P_{stack} \tag{2.8}$$

$$P_{variable} = 0.04 * P_{stack} \tag{2.9}$$

The parasitic losses can be expressed as following:

$$P_{parasitic} = P_{fixed} + P_{variable} \tag{2.10}$$

$$= V_{bmin}^2 * R_{fixed} + K * \left(\frac{I_{stack}}{SOC}\right) \tag{2.11}$$

Where:

- P_{fixed} : is the fixed losses.
- $P_{variable}$: is the variable losses.
- V_{bmin} : is the minimum battery voltage.
- R_{fixed} : is the fixed resistance.
- K : is a constant coefficient correlated with re-circulation pump power losses.

The constant coefficient correlated with re-circulation pump power losses are calculated at 20 % SOC and maximum battery current, so it can be expressed as following:

$$K = \frac{P_{variable} * SOC_{worse}}{I_{max}} \tag{2.12}$$

The fixed resistance can be calculated from equation 2.11 as following:

$$R_{fixed} = \frac{V_{bmin}^2}{P_{fixed}} \tag{2.13}$$

Also, the pump current can be calculated from equation 2.11 as following:

$$I_{pump} = \frac{P_{variable}}{V_{bmin}} \tag{2.14}$$

$$= \frac{K * \left(\frac{I_{stack}}{SOC}\right)}{V_{bmin}} \tag{2.15}$$

2.4.4 SOC Calculation

The system SOC can be defined as :

$$SOC = \left(\frac{CurrentEnergyinBattery}{TotalEnergyCapacity}\right) \tag{2.16}$$

The SOC is computed each cycle based on the previous SOC. SOC is updated periodically by accumulating electrical energy flowing through the battery stack.

$$SOC_{t+1} = SOC_t + \Delta SOC \tag{2.17}$$

$$\Delta SOC = \frac{\Delta E}{E_{capacity}} = \frac{P_{stack} * T_{Step}}{P_{rating} * T_{rating}} = \frac{I_{stack} * V_{stack} * T_{Step}}{P_{rating} * T_{rating}} \tag{2.18}$$

where:

- SOC_t : is the SOC at the instant of t.
- SOC_{t+1} : is the SOC at the instant of t+1.
- Δ SOC : is the change of the SOC in a time step Δ t it is positive during charge, negative during discharge.
- Δ E : is the energy change in a time step Δ t.

- $E_{capacity}$: is the battery total capacity.

- T_{rating} : is the time when battery total energy is charged into the battery at the battery power rating.

- T_{step} : is the time step.

The SOC can be implemented by using a discrete time integrator block by accumulation the values of previous SOC. It computed each cycle based on the previous SOC, depending on the input values [24].

2.4.5 Electrode Capacitor Calculation

The transient effects are related to electrode capacitance. Each cell is approximated to have a series capacitance of 6 Farad. The electrodes capacitance can be expressed as following:

$$C_{electrodes} = \frac{6}{n} \tag{2.19}$$

The parameters for the VRFB are in Table 2.2:

Table 2.2: VRFB Parameters

Parameter	Value	Units
Number of cells	230	Cell
Power rating	25	KW
Energy rating	50	KWh
Minimum Voltage	150	Volt
Maximum Current	166.6667	Amp
Operating Region	20-80	% SOC

The parameters for the equivalent circuit of the VRFB are in Table 2.3:

Table 2.3: Euivalent Circuit of the VRFB Parameters

Parameter	Value	Units
$C_{electrodes}$	0.0261	Farad
$R_{reaction}$	0.1025	Ohm
$R_{resistive}$	0.0684	Ohm
R_{fixed}	35.55	Ohm

2.5 Lithium-Ion Battery

The parameters for the LI-IB are in Table 2.4. The Model of LI-IB from MATLAB/SIMULINK ® is used.

Table 2.4: LI-IB Parameters

Parameter	Value	Units
Number of batteries	6	Batteries
Power rating	2.5	KW
Energy rating	2.2	KWh
Nominal Voltage	48	Volt
Capacity rating	45.8333	Ah
Minimum Voltage	42	Volt
Maximum Voltage	56	Volt
Operating Region	20-80	% SOC
Maximum Current	50	Amp

Chapter 3

Emulating the Batteries

3.1 Introduction

The VRFB and LI-IB battery will be emulated by a three phase rectifier and the dynamics of the battery will be implemented in the software to get more or less the behavior of the batteries . This way can be used for any technology of batteries.

3.2 Emulating the Batteries

A three phase rectifier is used to get the initial DC voltage of the batteries as shown in Figure 3-1 and Figure 3-2. A regulated DC source can be used instead of the three phase rectifier. Capacitors are used to decrease the ripples and smoothing the DC voltage. Charging resistance is used to charge the capacitor smoothly. Discharging resistance is used to discharge the capacitor and in case of the power flowing from the DC bus through the boost converter to the three phase rectifier or the regulated DC source. By using a battery, the power is flowing from and to the battery in charging and discharging modes respectively, the discharging resistance will behave the same in the case of charging the battery. The two circuits of the VRFB and the LI-IB are the same but the difference in the value of the voltage of three phase source or the voltage of the regulated DC source. A regulated DC source is used. The three phase rectifier will be used in future development.

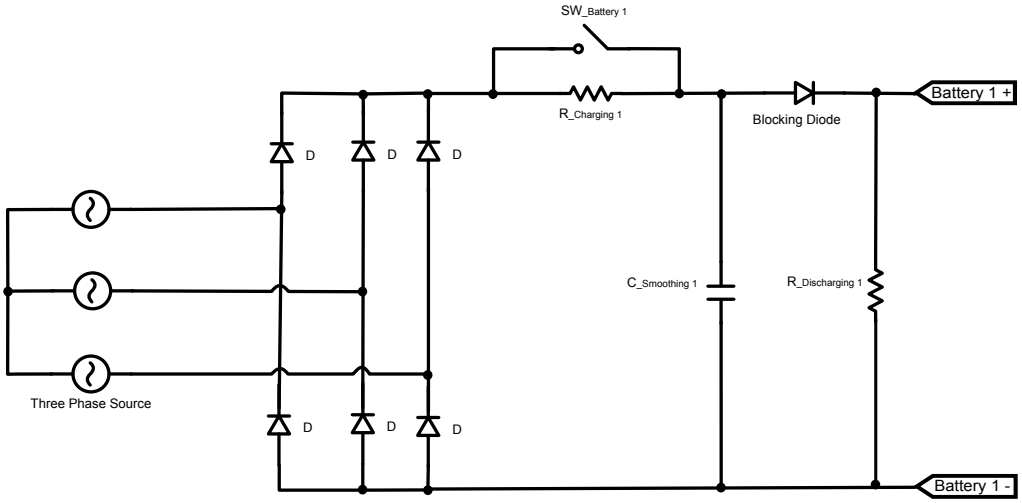

Figure 3-1: Emulating of VRFB.

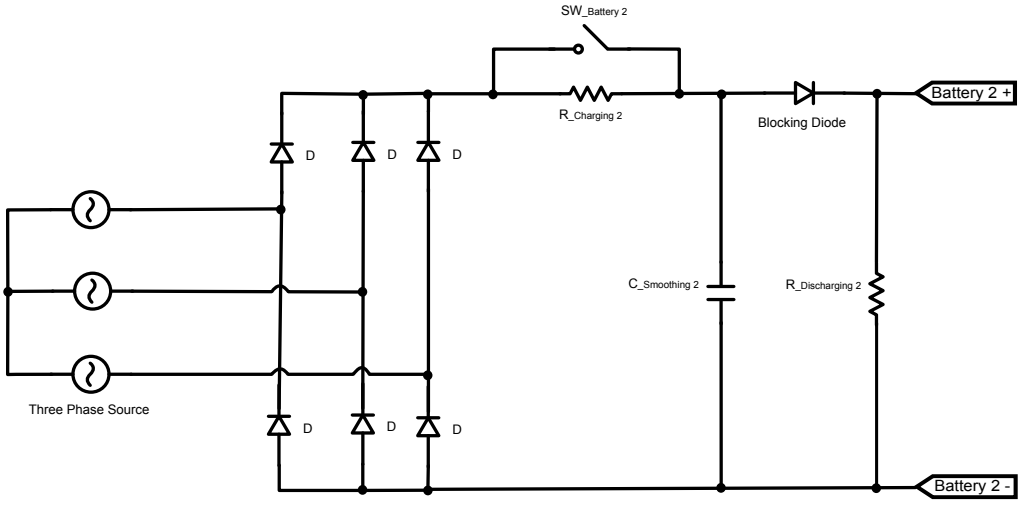

Figure 3-2: Emulating of LI-IB.

3.3 Emulating the Dynamics of the Batteries

The dynamic behavior of any battery can be represented by the circuit consists of series resistor, SOC capacitor, dynamic capacitor and dynamic resistance [27] as shown in Figure 3-3.

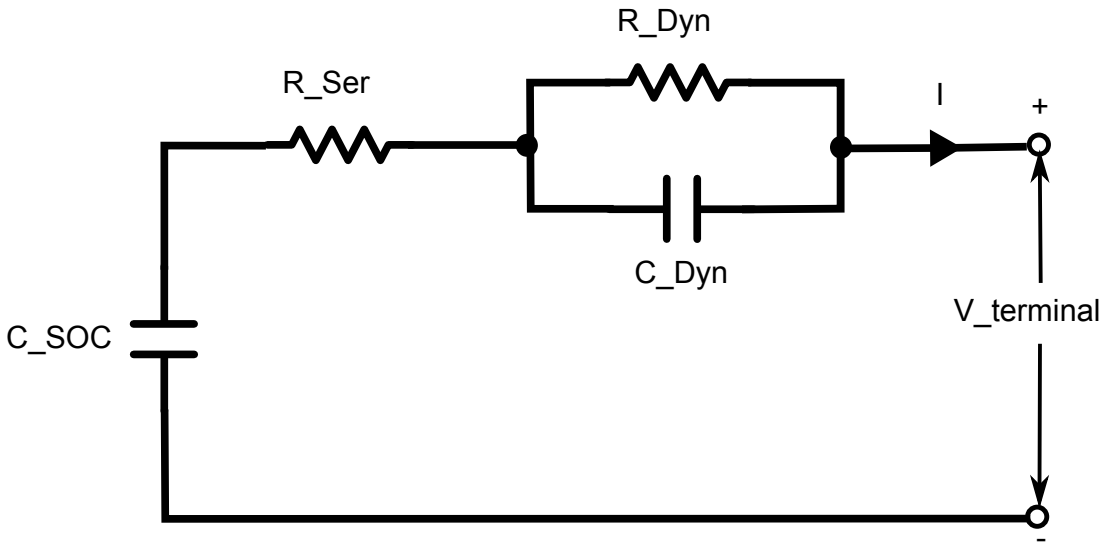

Figure 3-3: Dynamic behavior equivalent circuit of any battery.

The transfer function of the equivalent circuit is:

$$TF = \frac{V_{initial} - V_{terminal}}{I} \tag{3.1}$$

where

- $V_{initial}$: is the initial condition of the Capacitor C_{SOC}.

$$= -\frac{R_{ser} * s^2 + \left(\frac{1}{C_{SOC}} + \frac{1}{R_{Dyn} * C_{Dyn}} * R_{ser} + \frac{1}{C_{Dyn}}\right) * s + \frac{1}{R_{Dyn} * C_{Dyn}} * \frac{1}{C_{SOC}}}{s^2 + \frac{1}{R_{Dyn} * C_{Dyn}} * s} \tag{3.2}$$

The negative sign is because the current is considered positive flowing out from the battery. This transfer function is implemented in the DSP to get the virtual battery voltage. The virtual voltage of VRFB and LI-IB is calculated as shown in

Figure 3-4. The virtual voltage has more or less the dynamics of the real battery voltage. This model could be easily converted to a model with variable coefficients, to continuously adapt the dynamic behavior of the batteries to the SOC. It will be done in the future development.

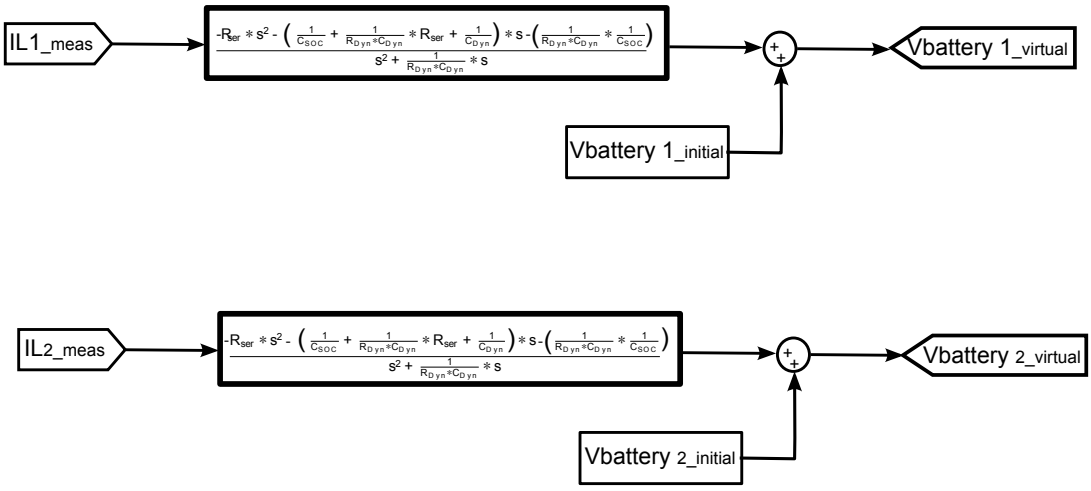

Figure 3-4: Virtual voltage calculation for VRFB and LI-IB.

The parameters of the dynamic equivalent circuit is calculated as following by applying a current step to the battery:

At the current step, an instant voltage step appear. The series resistance is calculated at the point which the current step changes as following:

$$R_{ser} = \frac{\Delta V}{\Delta I} \tag{3.3}$$

After the current step, an exponential response is found at the voltage. The dynamic resistor and the dynamic capacitor are calculated as following:

$$R_{dyn} = \frac{\Delta V}{\Delta I} \tag{3.4}$$

$$C_{dyn} = \frac{Ts}{3 * R_{dyn}} \tag{3.5}$$

The SOC capacitor is calculated as following:

$$I = C_{SOC} * \frac{\Delta V}{\Delta t} \tag{3.6}$$

$$C_{SOC} = \frac{I}{\frac{\Delta V}{\Delta t}} \tag{3.7}$$

3.3.1 Emulating the Dynamics of the VRFB

To calculate the parameters of the dynamic equivalent circuit, a current step; i.e., from -10 A to -60 A) is applied to to the VRFB model implemented in chapter 2 in MATLAB/SIMULINK ® to get the voltage profile as shown in Figure 3-5. Figure 3-6 is a zoom of Figure 3-5.

The parameters of the dynamic equivalent circuit of VRFB are calculated by using equations 3.3, 3.4, 3.5 and 3.7 and the values are in Table 3.1:

Table 3.1: Dynamic Equivalent Circuit of the VRFB Parameters

Parameter	Value	Units
R_{ser}	0.06826	Ohm
C_{SOC}	7594.93	Farad
C_{Dyn}	0.025	Farad
R_{Dyn}	0.0996	Ohm
V_{init}	302.429	Volt

3.3.2 Emulating the Dynamics of the LI-IB

Also, to calculate the parameters of the dynamic equivalent circuit of the LI-IB, a current step; i.e., from -10 A to -20 A is applied to to the LI-IB model of

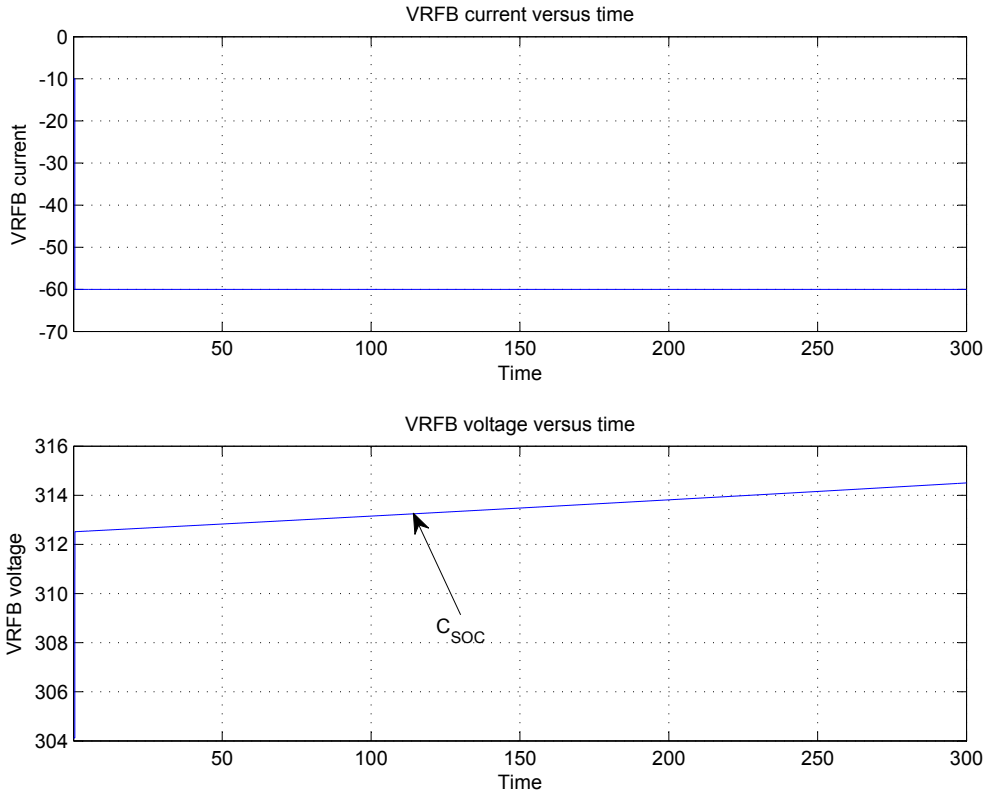

Figure 3-5: VRFB virtual voltage.

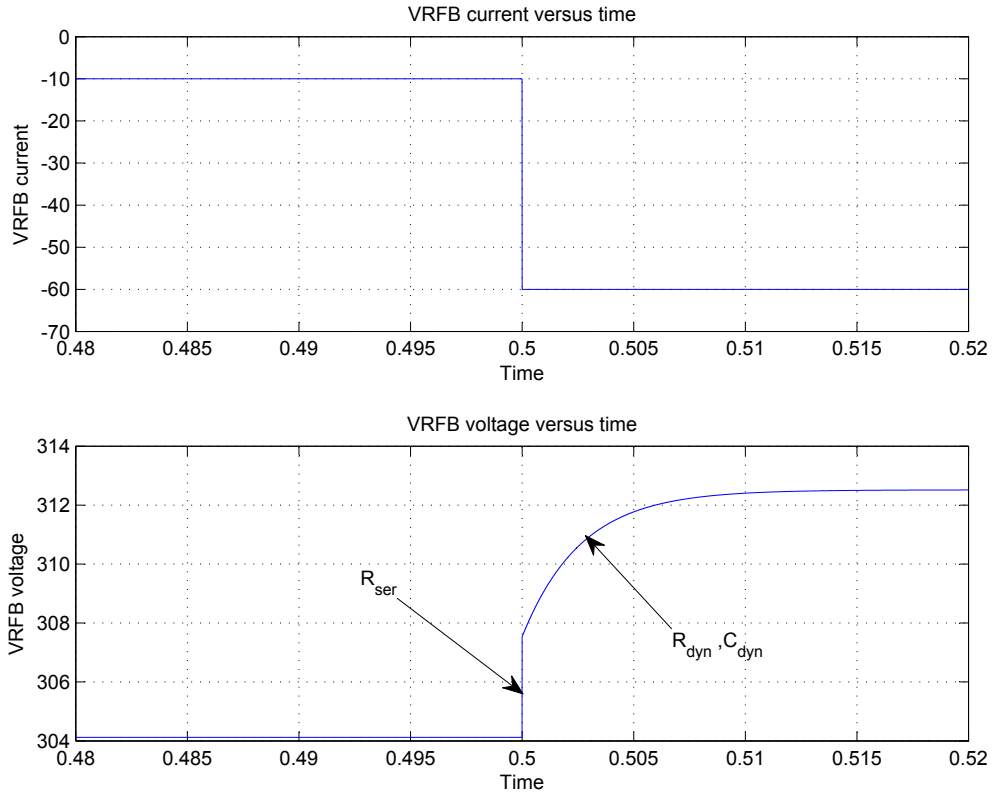

Figure 3-6: Zoom at VRFB virtual voltage.

MATLAB/SIMULINK ® to get the voltage profile as shown in Figure 3-7. Figure 3-8 is a zoom of Figure 3-7.

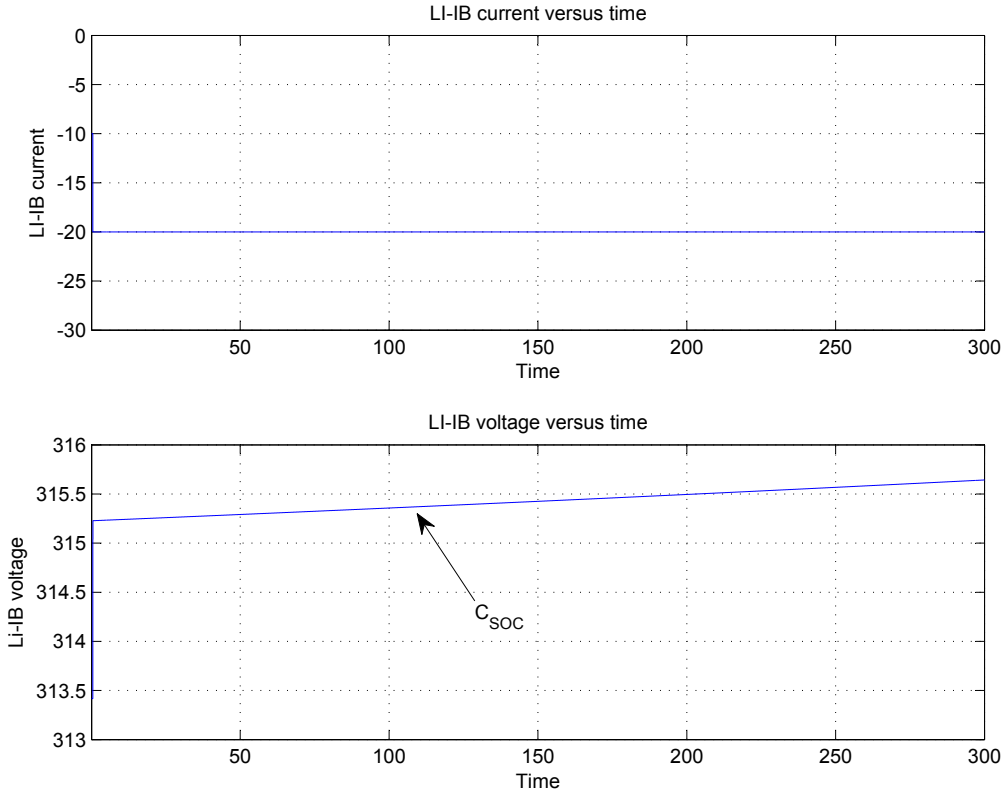

Figure 3-7: LI-IB virtual voltage.

The parameters of the dynamic equivalent circuit of LI-IB are calculated by using equations 3.3, 3.4, 3.5 and 3.7 and the values are in Table 3.2:

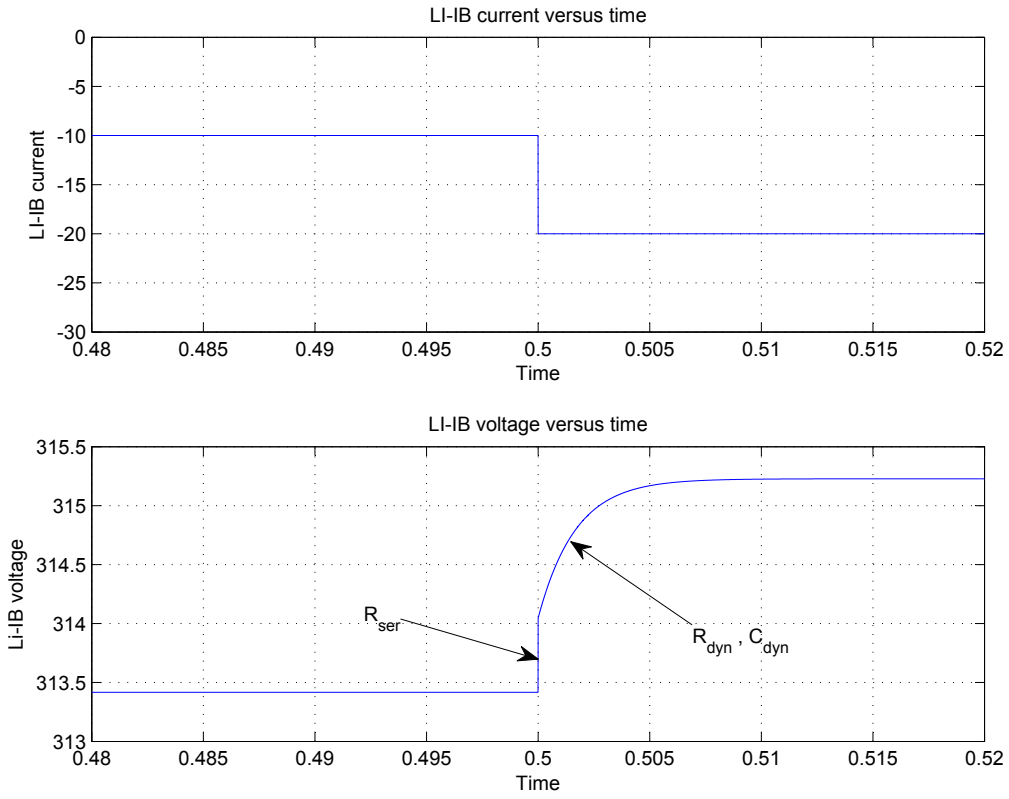

Figure 3-8: Zoom at LI-IB virtual voltage.

Table 3.2: Dynamic Equivalent Circuit of the LI-IB Parameters

Parameter	Value	Units
R_{ser}	0.0628	Ohm
C_{SOC}	14106	Farad
C_{Dyn}	0.0127	Farad
R_{Dyn}	0.1181	Ohm
V_{init}	311.6	Volt

Chapter 4

Control of the Two Converters

4.1 Introduction

The system has two bidirectional boost converters. Every bidirectional boost converter has his own control. The control of the second boost converter is dependent on the first control. One converter is controlling the DC bus voltage to avoid stability problems [28] and the other converter is controlling the peak transient power when load changes suddenly. The power circuit of the system is shown in Figure 4-1.

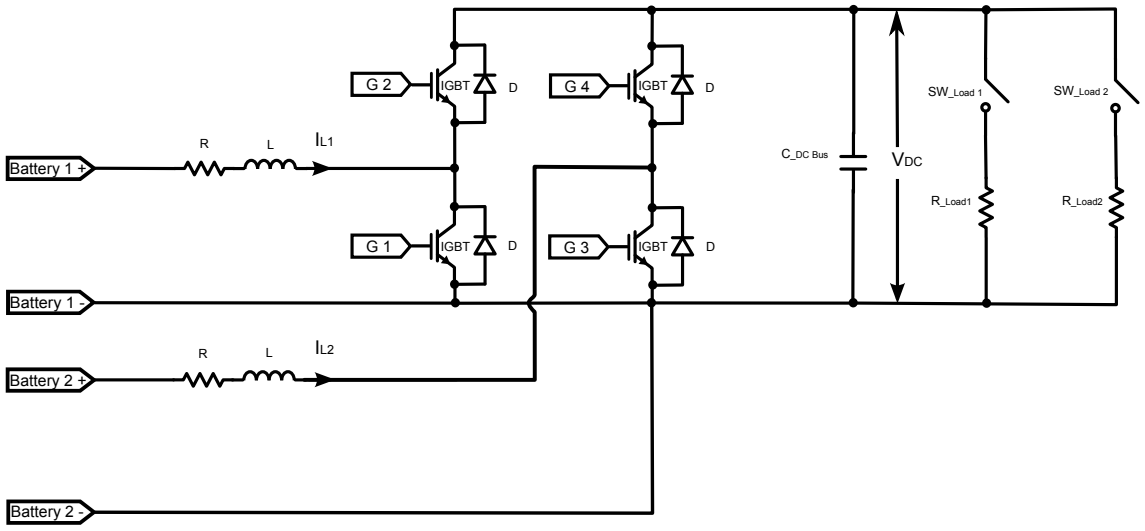

Figure 4-1: The power circuit of the system.

The parameters of the power circuit are in Table 4.1

Table 4.1: Power Circuit Parameters

Parameter	Value	Units
Resistance of the inductor	1	Ohm
Inductance of the inductor	0.042	Henry
DC bus capacitance	1000	μ Farad
Load 1	300	Ohm
Load 2	300	Ohm

The inductor value has to calculated to have a small current ripple because the current ripple will result in battery heating, as well as increased battery cycling, which can have a negative impact on the battery life [7].

4.2 Control of First Boost Converter

The control of the first boost converter is to keep the DC bus voltage constant around 600 Volt. There two control loops, the outer control loop is DC bus voltage control loop and the inner control loop is the inductor current control loop [26], [5], [28], [29], [30], [23] as shown in Figure 4-2.

The inductor current control loop has to be faster than the DC bus voltage control loop. The bandwidth of the inductor current control is 300 Hz, the bandwidth of the DC bus voltage control is 30 Hz.

4.2.1 DC Bus Voltage Control Loop

PI control will be used to control the DC bus voltage to be around 600 volt.

$$PI\left(s\right) \quad = \quad K_{P_v} * \left(\frac{s + \frac{1}{T_i}}{s} \right) \tag{4.1}$$

Using zero pole cancellation method for tuning the parameters of the PI control

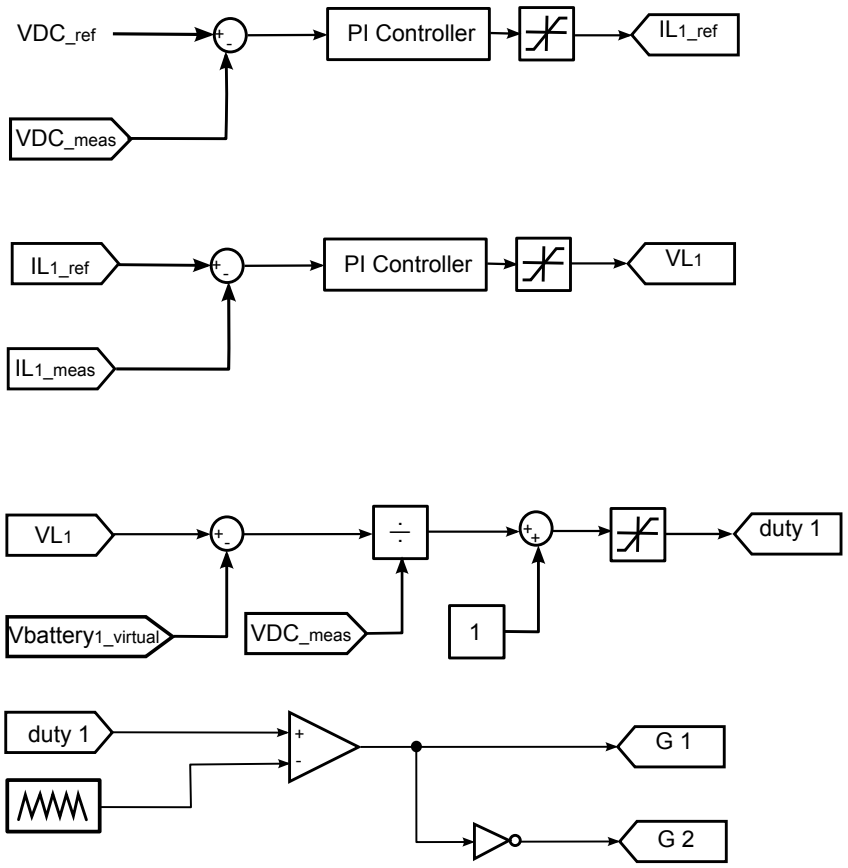

Figure 4-2: Control of first bidirectional boost converter.

with a bandwidth of 30 Hz, the PI parameters are:

$$K_{P_v} = 2 * Pi * Bw_v * C_{DC_{Bus}} \quad (4.2)$$

$$= 2 * Pi * 30 * 1000 * 10^{-6} = 0.1885 \quad (4.3)$$

$$T_{i_v} = C_{DC_{Bus}} * R_{Load} \quad (4.4)$$

$$= 1000 * 10^{-6} * 300 = 0.3 \quad (4.5)$$

The reference DC bus voltage is obtained 600 volt. The input to the controller is the error and it is equal to the difference between the reference DC bus voltage and the measured DC bus voltage. The upper and lower limits of the output of the controller which is the reference current is depending on the maximum and minimum current of the VRFB during charging and discharging.

To avoid the windup due to the limits of current, anti windup technique has to be implemented. The controller output has to be between these upper and lower limits and the error has to be calculated again if the output controller exceeds or below these limits.

4.2.2 Inductor Current Control Loop

PI control will be used also to control the inductor current. Using also zero pole cancellation method for tuning the parameters of the PI control with a bandwidth of 300 Hz, the PI parameters are:

$$K_{P_i} = 2 * Pi * Bw_i * L_{inductor} \quad (4.6)$$

$$= 2 * Pi * 300 * 42 * 10^{-3} = 79.1681 \quad (4.7)$$

$$T_{i_v} = \frac{L_{inductor}}{R_{inductor}} \quad (4.8)$$

$$= \frac{42 * 10^{-3}}{1.0} = 0.042 \quad (4.9)$$

The reference current of inductor is obtained from DC bus voltage control loop. The input to the controller is the error and it is equal to the difference between the reference inductor current and the measured inductor current. The limits of the output of the controller which is the voltage across the inductor is determined by:

$$V_{L_{1_{min}}} = V_{Bat._1} - V_{DC_{Bus}} \tag{4.10}$$

$$V_{L_{1_{max}}} = V_{Bat._1} \tag{4.11}$$

To avoid the windup due to the limits of the voltage across the inductor, anti windup technique has to be implemented. The controller output has to be between these upper and lower limits and the error has to be calculated again if the output controller exceeds these limits.

4.2.3 Duty Cycle Calculation

The switching frequency of the IGBT is 10 KHz. The duty cycle of the IGBT is calculated as following:

$$V_{Bat.virtual_1} - (1 - d_1) * V_{DC_{Bus}} = V_{L_1} \tag{4.12}$$

$$V_{Bat.virtual_1} - V_{L_1} = (1 - d_1) * V_{DC_{Bus}} \tag{4.13}$$

$$\frac{V_{Bat.virtual_1} - V_{L_1}}{V_{DC_{Bus}}} = (1 - d_1) \tag{4.14}$$

$$d_1 = 1 - \frac{V_{Bat.virtual_1} - V_{L_1}}{V_{DC_{Bus}}} \tag{4.15}$$

$$d_1 = 1 + \frac{V_{L_1} - V_{Bat.virtual_1}}{V_{DC_{Bus}}} \tag{4.16}$$

The limits of the duty cycle is:

$$d_{1_{min}} = 0 \tag{4.17}$$

$$d_{1_{max}} = 1 \tag{4.18}$$

The duty cycle is then compared with the carrier to generate the switching signals. This duty cycle for switching IGBT 1 and the complementary signal for switching IGBT 2.

4.3 Control of Second Boost Converter

The control of the second boost converter to provide the peak transient power when the load changes suddenly. This control will accelerate the recovery of reduction in the voltage fall of the DC bus voltage. There two control loops, the outer control loop is power control loop and the inner control loop is the inductor current control loop [9], [30] as shown in Figure 4-3.

The inductor current control loop has to be faster than the power control loop. The bandwidth of the inductor current control is 300 Hz.

4.3.1 Power Control Loop

PI control will be used also to control the power of the LI-IB. Using trial and error method for tuning the parameters of the PI control [31], the PI parameters are:

$$K_{P_p} = 1.558 \tag{4.19}$$

$$T_{i_p} = 1 \tag{4.20}$$

The reference power of LI-IB is obtained from the difference between the power of the VRFB and the power of the VRFB filtered by a Low pass filter to obtain the low frequency part or from the difference betwween the power from load and the power from the load filtered by a low pass filter to obtain the low frequency part [1], [2], [4], [9], [31], [32], [33]. The first method is used and the second method will be used in the future development to select the optimal method to create the reference power. If the frequency of the filter decreases , the reference power reference increases. The value selected of the frequency of the filter is 10 Hz. The input to the controller is the error and it is equal to the difference between the reference LI-IB power and the

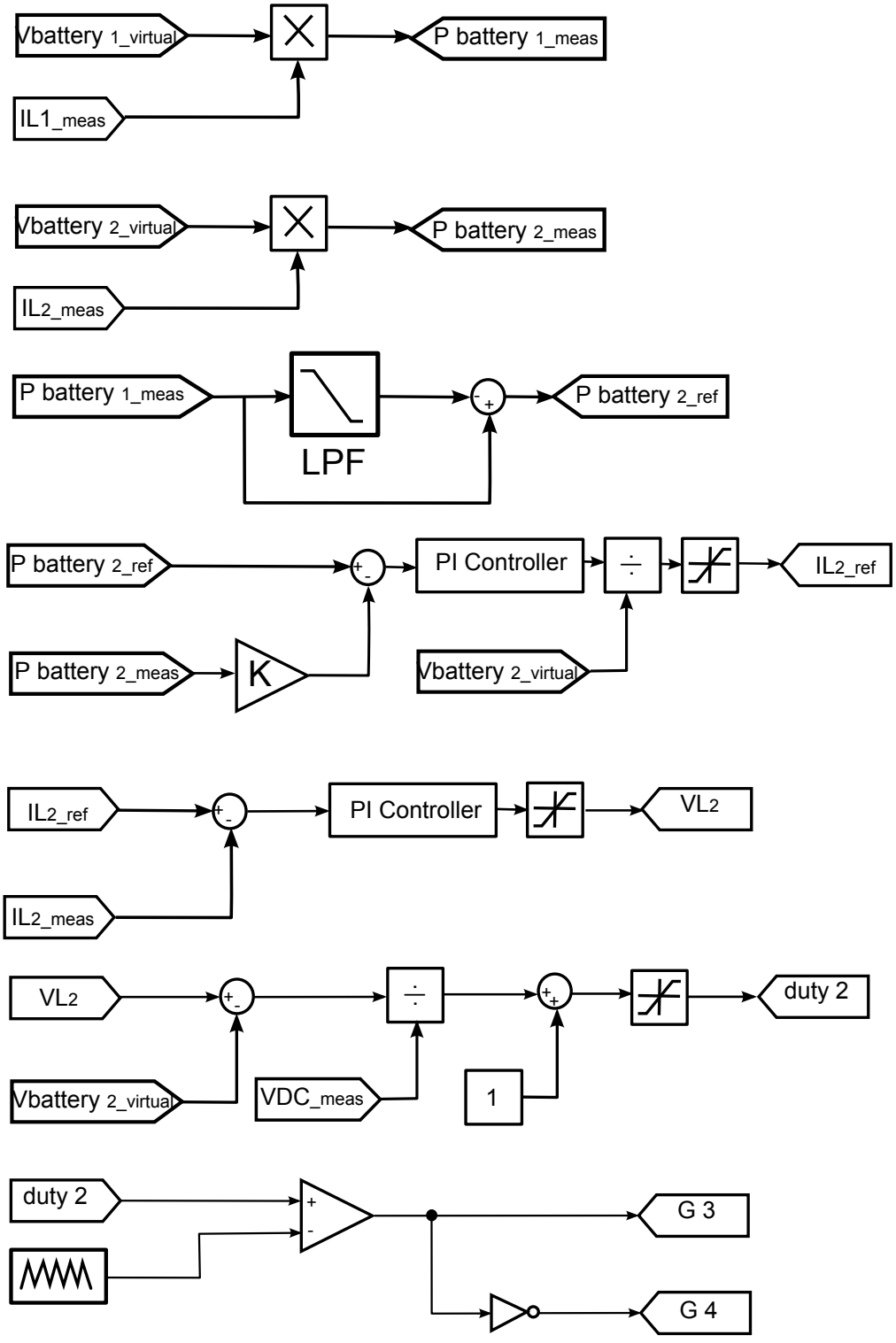

Figure 4-3: Control of second bidirectional boost converter.

measured LI-IB power multiplied by K to increase the power of LI-IB when changing the controllable load 2 [28]. This means that more power will be released when encountered with a sudden load, which will be helpful for the recovering of the DC voltage. The limits of the output of the controller which is the power is determined by the power that LI-IB can supply.

To avoid the windup due to the limits of the power, anti windup technique has to be implemented. The controller output has to be between these upper and lower limits and the error has to be calculated again if the output controller exceeds these limits.

4.3.2 Inductor Current Control Loop

PI control will be used also to control the inductor current. Using also zero pole cancellation method for tuning the parameters of the PI control with a bandwidth of 300 Hz, the PI parameters are the same as the PI parameters of the inductor current control loop of the first boost converter as the inductors have the same values.

The reference current of inductor is obtained from power control loop divided by the LI-IB virtual voltage. The input to the controller is the error and it is equal to the difference between the reference inductor current and the measured inductor current. The limits of the output of the controller which is the voltage across the inductor is determined by:

$$V_{L_{2_{min}}} = V_{Bat.2} - V_{DC_{Bus}} \tag{4.21}$$

$$V_{L_{2_{max}}} = V_{Bat.2} \tag{4.22}$$

To avoid the windup due to the limits of the voltage across the inductor, anti windup technique has to be implemented. The controller output has to be between these upper and lower limits and the error has to be calculated again if the output controller exceeds these limits.

4.3.3 Duty Cycle Calculation

The switching frequency of the IGBT is 10 KHz. The duty cycle of the IGBT is calculated as following:

$$V_{Bat.virtual_2} - (1 - d_2) * V_{DC_{Bus}} = V_{L_2} \tag{4.23}$$

$$V_{Bat.virtual_2} - V_{L_2} = (1 - d_2) * V_{DC_{Bus}} \tag{4.24}$$

$$\frac{V_{Bat.virtual_2} - V_{L_2}}{V_{DC_{Bus}}} = (1 - d_2) \tag{4.25}$$

$$d_2 = 1 - \frac{V_{Bat.virtual_2} - V_{L_2}}{V_{DC_{Bus}}} \tag{4.26}$$

$$d_2 = 1 + \frac{V_{L_2} - V_{Bat.virtual_2}}{V_{DC_{Bus}}} \tag{4.27}$$

The limits of the duty cycle is:

$$d_{2_{min}} = 0 \tag{4.28}$$

$$d_{2_{max}} = 1 \tag{4.29}$$

The duty cycle is then compared with the carrier to generate the switching signals. This duty cycle for switching IGBT 3 and the complementary signal for switching IGBT 4.

Chapter 5

Results

5.1 Introduction

This chapter presents the evaluation of the behavior of the designed HESS, by means of simulations and emulations in the laboratory setup. The simulations to test the model behavior have been carried in the MATLAB/SIMULINK ® environment. In these simulations, as well as in the emulation, the behavior of the HESS is studied and validated upon power variations. These steep power fluctuations take into account the stochastic behavior of renewable sources and load variations in microgrids.

5.2 Simulation Results

In all cases, the first controllable load is connected from the beginning of the simulation and the second load is connected and disconnected again to check the effect on the DC bus voltage. This connection and disconnection of the second load change the load power from 1200 Watt to 2400 Watt. The inductor current 1 is the same as the VRFB current and inductor current 2 is the same as the LI-IB current.

5.2.1 VRFB Only

The VRFB is connected to the DC bus and the controllable loads through Bidirectional Boost converter. In this case, LI-IB didn't taken into account.

The DC bus voltage decreased and VRFB current increased when controllable load 2 is connected, the DC bus voltage increased and VRFB current decreased when controllable load 2 is disconnected as shown in Figure 5-1 from simulation . Figure 5-2 is a zoom of Figure 5-1. When the controllable load 2 is disconnected, The virtual voltage of the VRFB will decrease again in the steady state but Figure 5-2 shows the transient only.

5.2.2 VRFB and LI-IB

The VRFB and LI-IB are connected to the DC bus and the controllable loads through the two Bidirectional Boost converter. Several parameter of the HESS have been changed, in order to check that the emulator and the simulations match at every condition.

K value in Figure 4-3 and the frequency of the low pass filter in Figure 4-3 of the power control loop of the second bidirectional converter will change to check the effect on the DC bus and the LI-IB current.

Case 1 : K = 1.0 and f_{lpf} = 10 Hz

The voltage drop in the DC bus and the over voltage are decreased compared to the previous case as shown in Figure 5-3 and in Table 5.1 due to using LI-IB as the peak transient current is drawing from the LI-IB. Figure 5-4 is a zoom of Figure 5-3.

Case 2 : K = 0.7 and f_{lpf} = 10 Hz

By decreasing the k, the voltage drop and the over voltage is decreased more and the LI-IB current is increased as shown in Figure 5-5 and Tables 5.1 and 5.2. Figure 5-6 is a zoom of Figure 5-5.

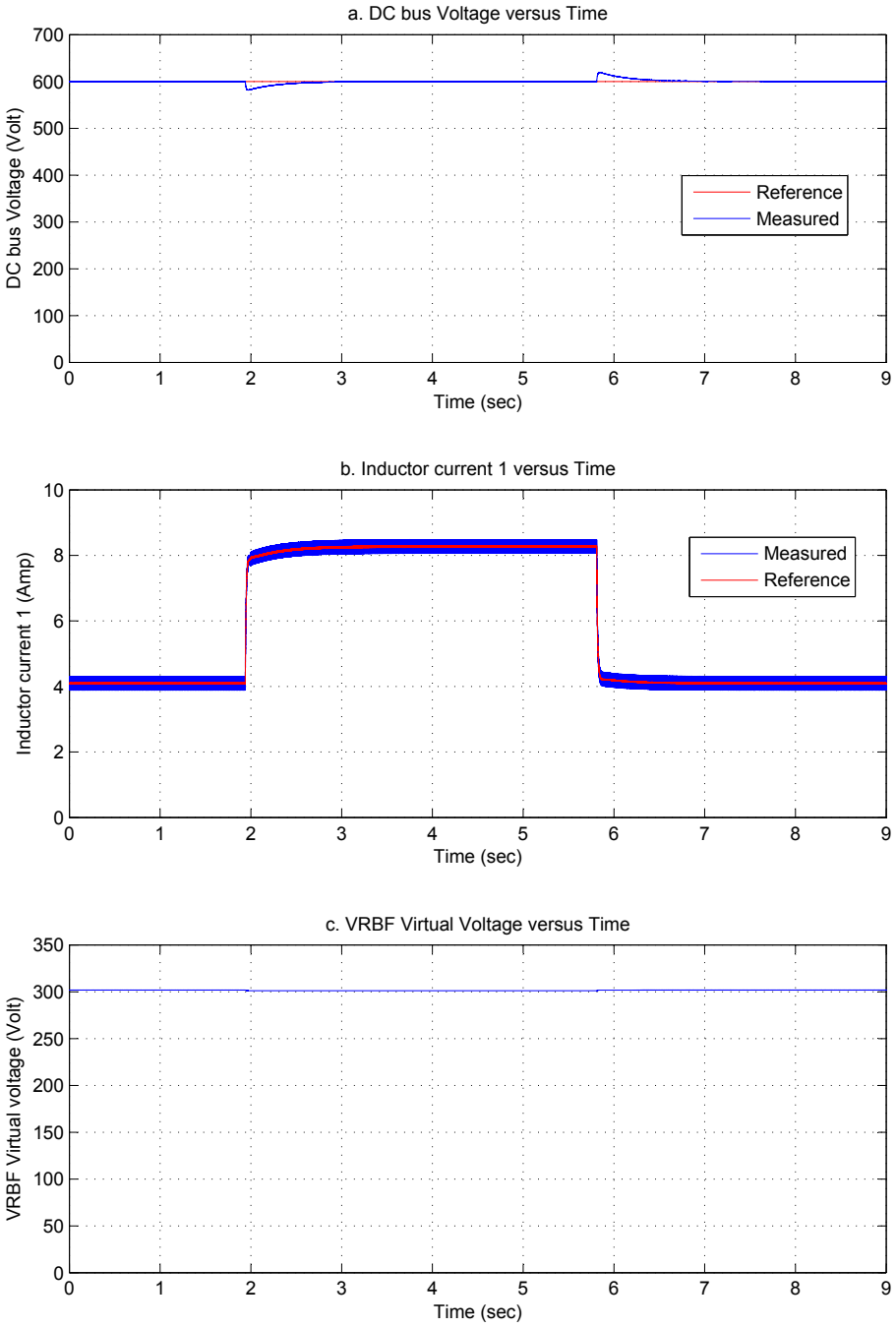

Figure 5-1: Simulation results without LI-IB: a. DC bus voltage. b. VRFB current. c. Virtual VRFB voltage.

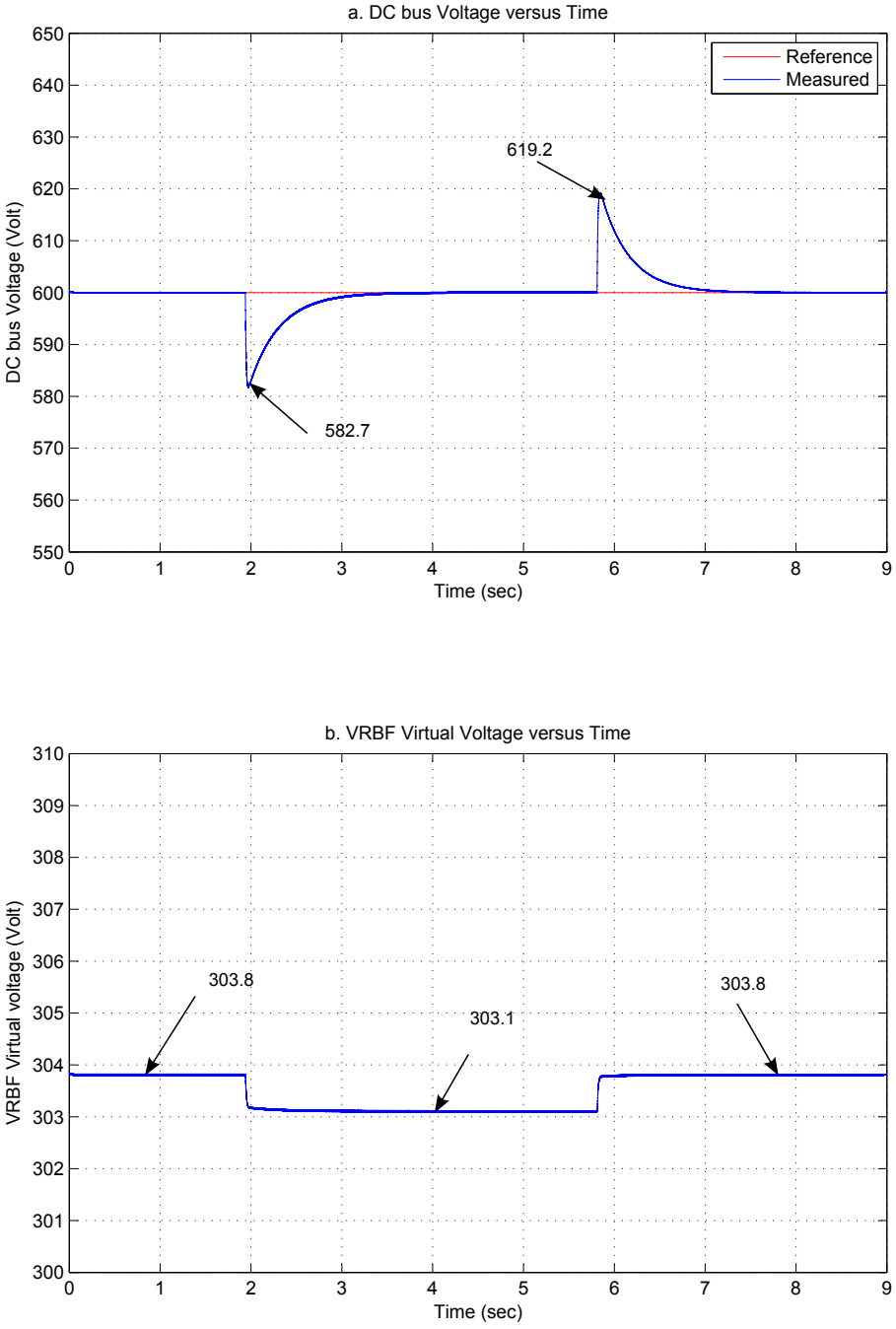

Figure 5-2: Simulation results without LI-IB: a. DC bus voltage. b. Virtual VRFB voltage.

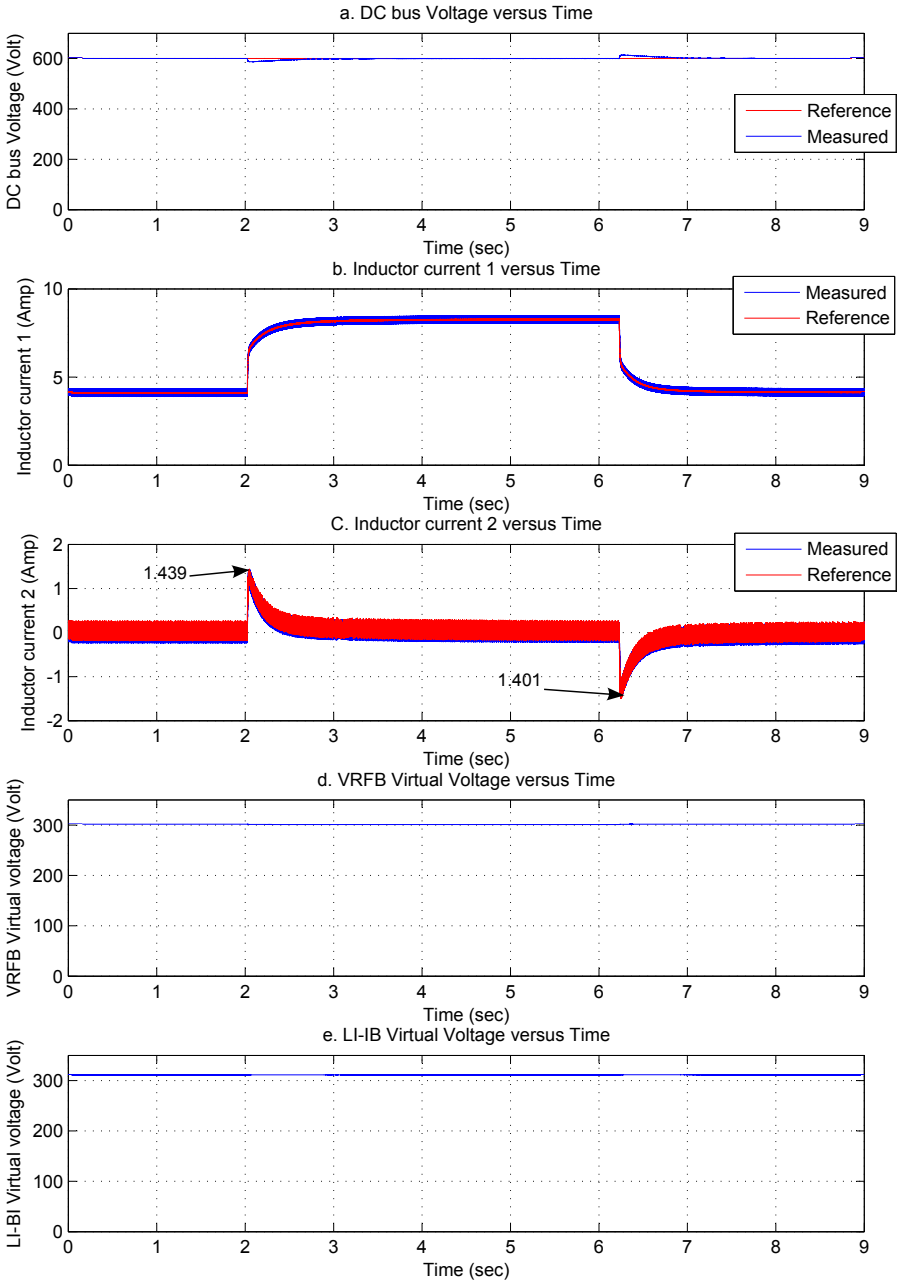

Figure 5-3: Simulation results at k = 1.0 and f_{lpf} = 10 Hz: a. DC bus voltage. b. VRFB current. c. LI-IB current. d. Virtual VRFB voltage. e. Virtual LI-IB voltage.

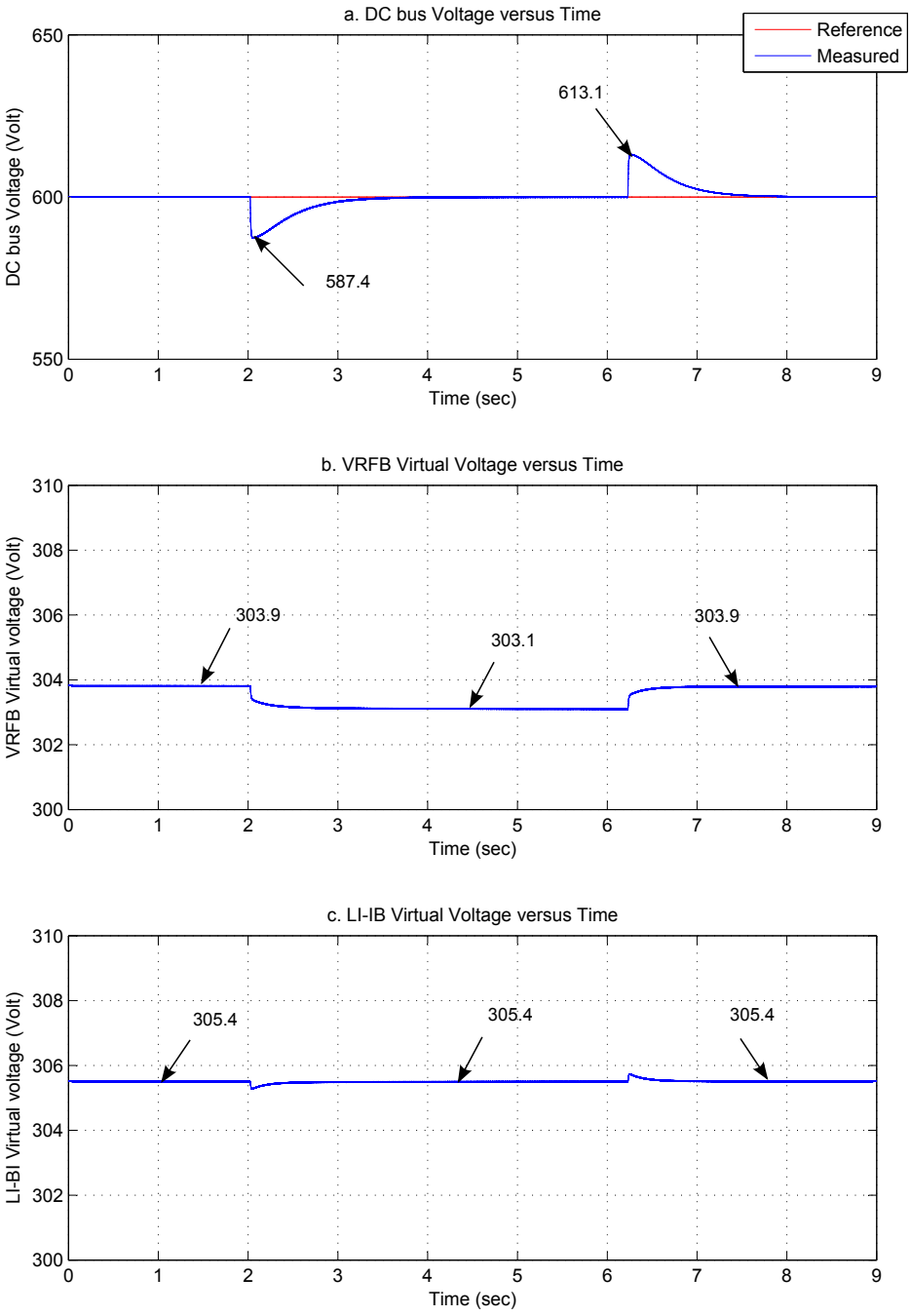

Figure 5-4: Simulation results at k = 1.0 and f_{lpf} = 10 Hz: a. DC bus voltage. b. Virtual VRFB voltage. c. Virtual LI-IB voltage.

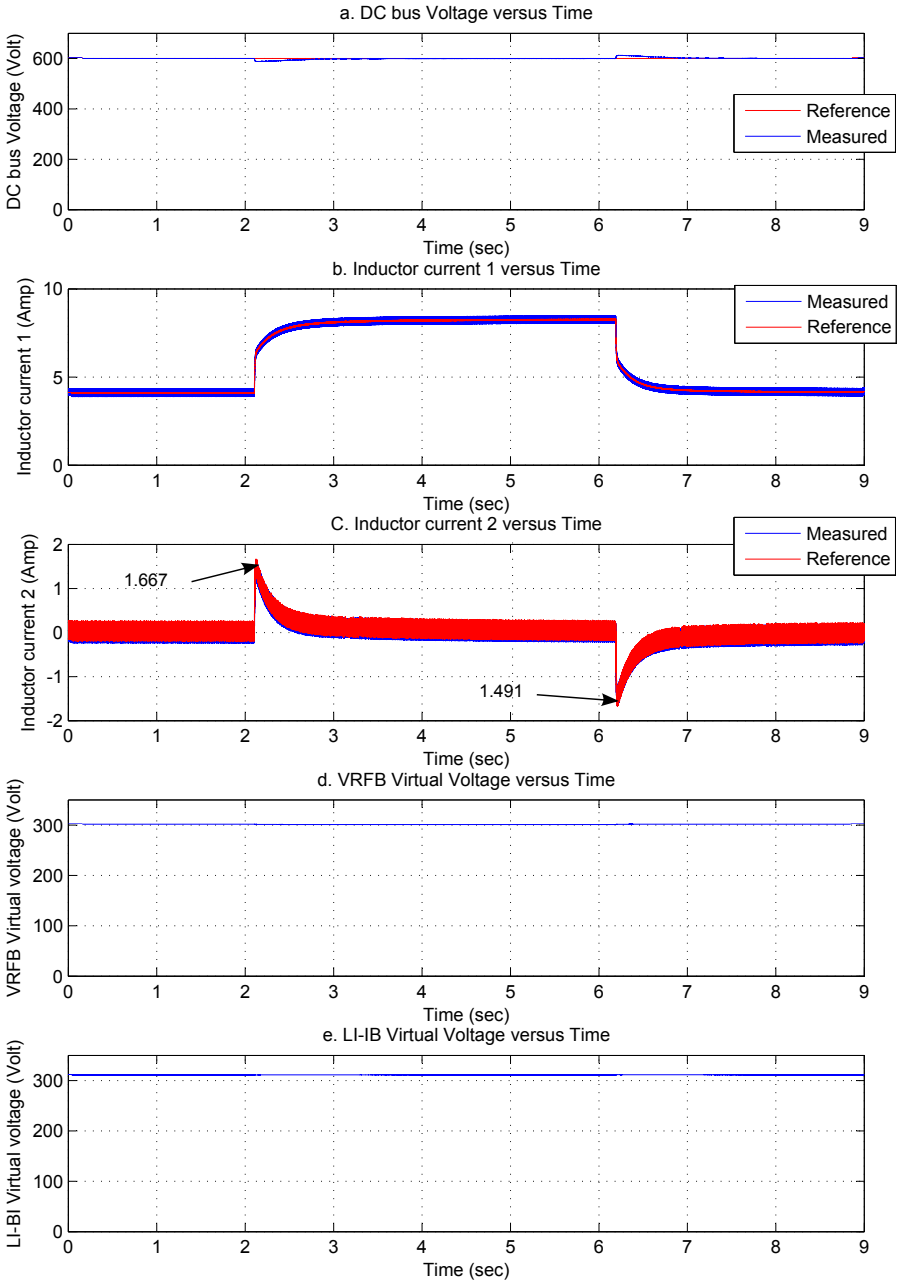

Figure 5-5: Simulation results at k = 0.7 and f_{lpf} = 10 Hz: a. DC bus voltage. b. VRFB current. c. LI-IB current. d. Virtual VRFB voltage. e. Virtual LI-IB voltage.

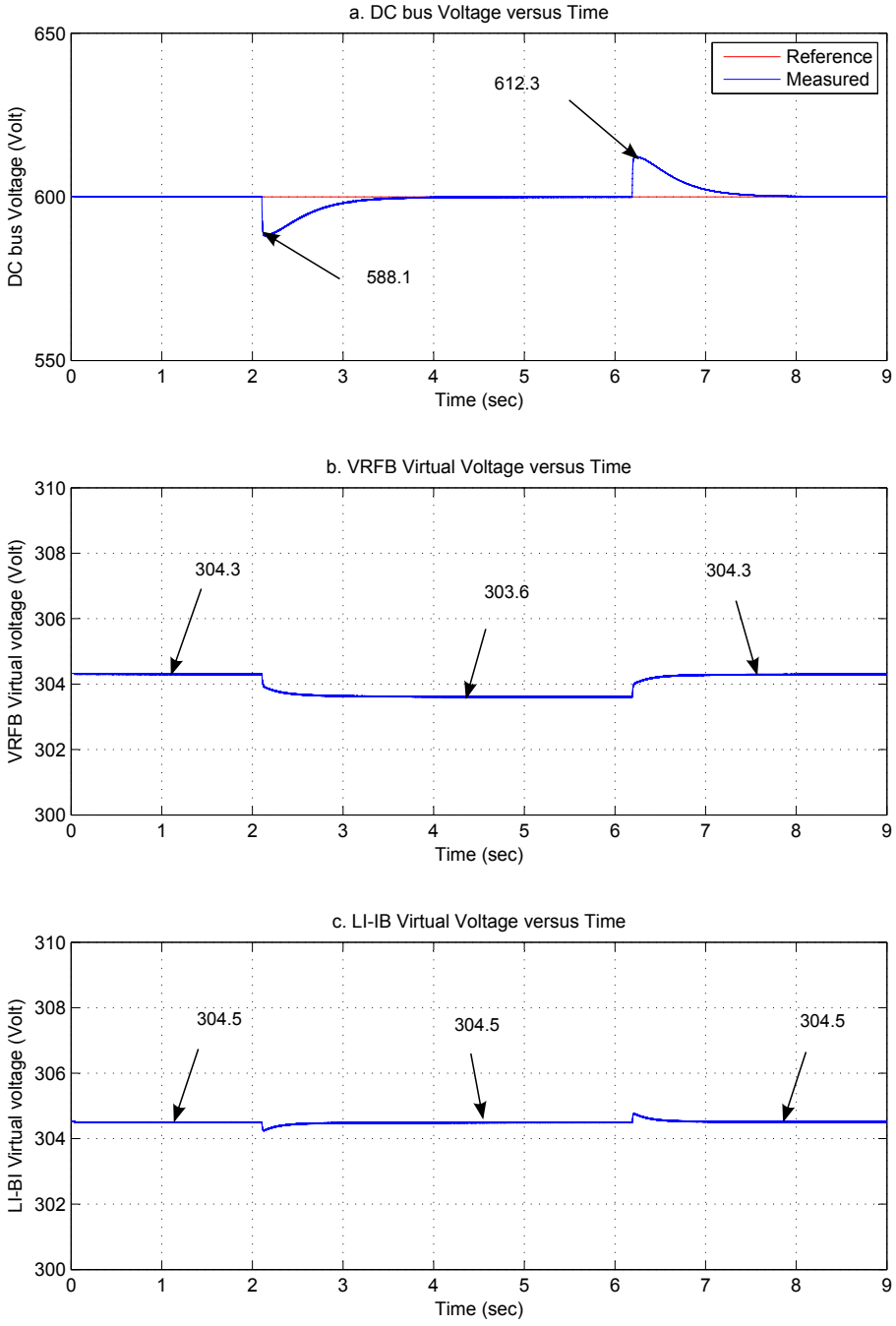

Figure 5-6: Simulation results at k = 0.7 and f_{lpf} = 10 Hz: a. DC bus voltage. b.Virtual VRFB voltage c.Virtual LI-IB voltage.

Table 5.1: DC Bus Voltage from Simulation Results

K	LPF frequency (Hz)	DC bus voltage when load 2 connected (Volt)	DC bus voltage when load 2 disconnected (Volt)
Without LI-IB	Without LI-IB	582.7	619.2
1.0	10	587.4	613.1
0.7	10	588.1	612.3

Table 5.2: LI-IB Current from Simulation Results

K	LPF frequency (Hz)	LI-IB Current when Load 2 connected (Amp)	LI-IB Current when load 2 disconnected (Amp)
1.0	10	1.439	1.401
0.7	10	1.667	1.491

5.3 Experimental Results (Emulation of the Batteries)

The control algorithm is implemented in the DSP. The cases of the simulations are validated by experiments and the frequency of the low pass filter is also changed.

5.3.1 VRFB Only

Figures 5-7 and 5-8 are compared to Figures 5-1 and 5-2. The DC bus voltage decreased and the VRFB current increased when controllable load 2 connected and the DC bus voltage increased and the VRFB current decreased when controllable load 2 disconnected. The results of the experiments are equal to the results of the simulation but the resolution of the virtual voltage of VRFB is very low due to this signal is coming from the DSP.

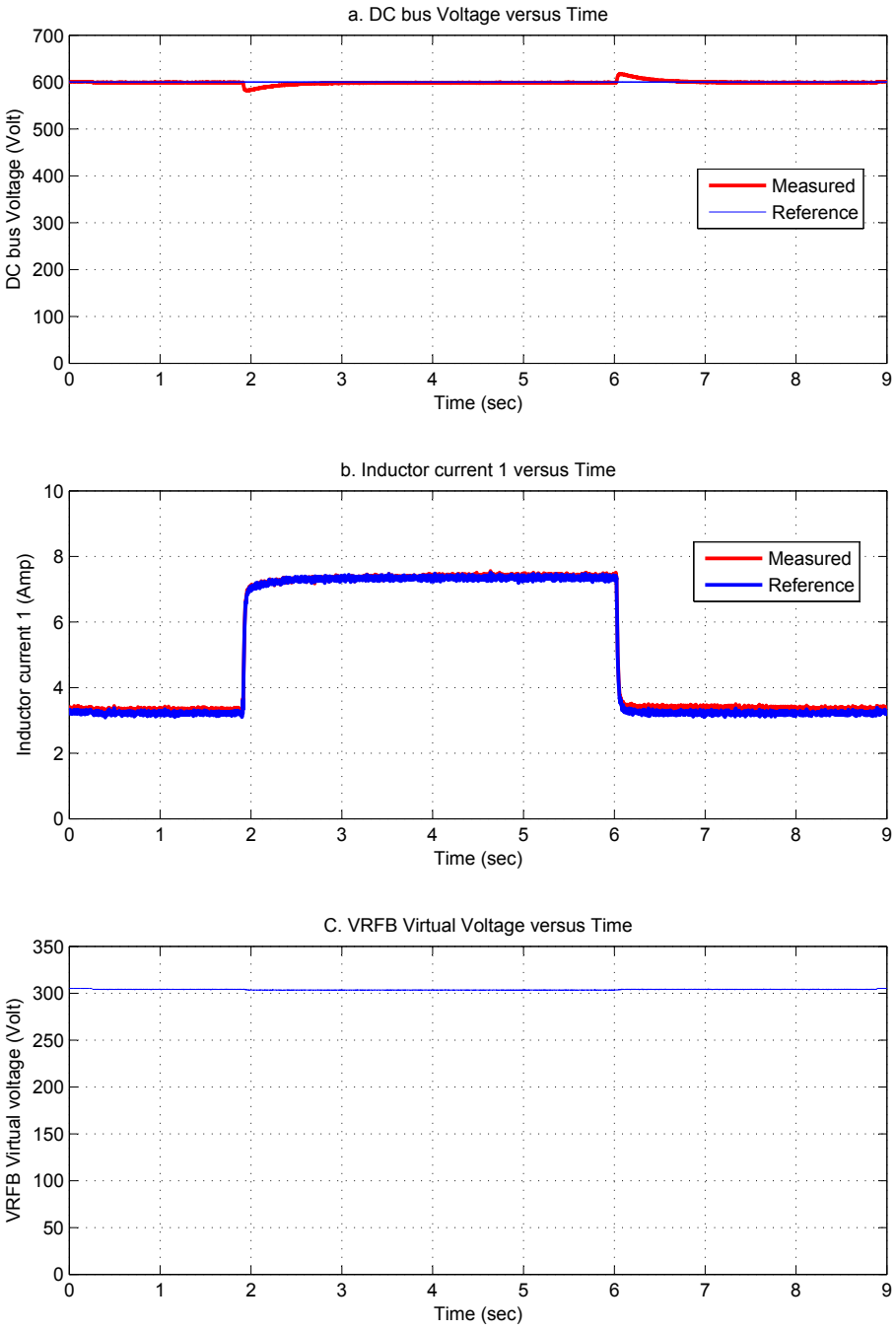

Figure 5-7: Experiments results without LI-IB: a. DC bus voltage. b. VRFB Current. c. Virtual VRFB voltage.

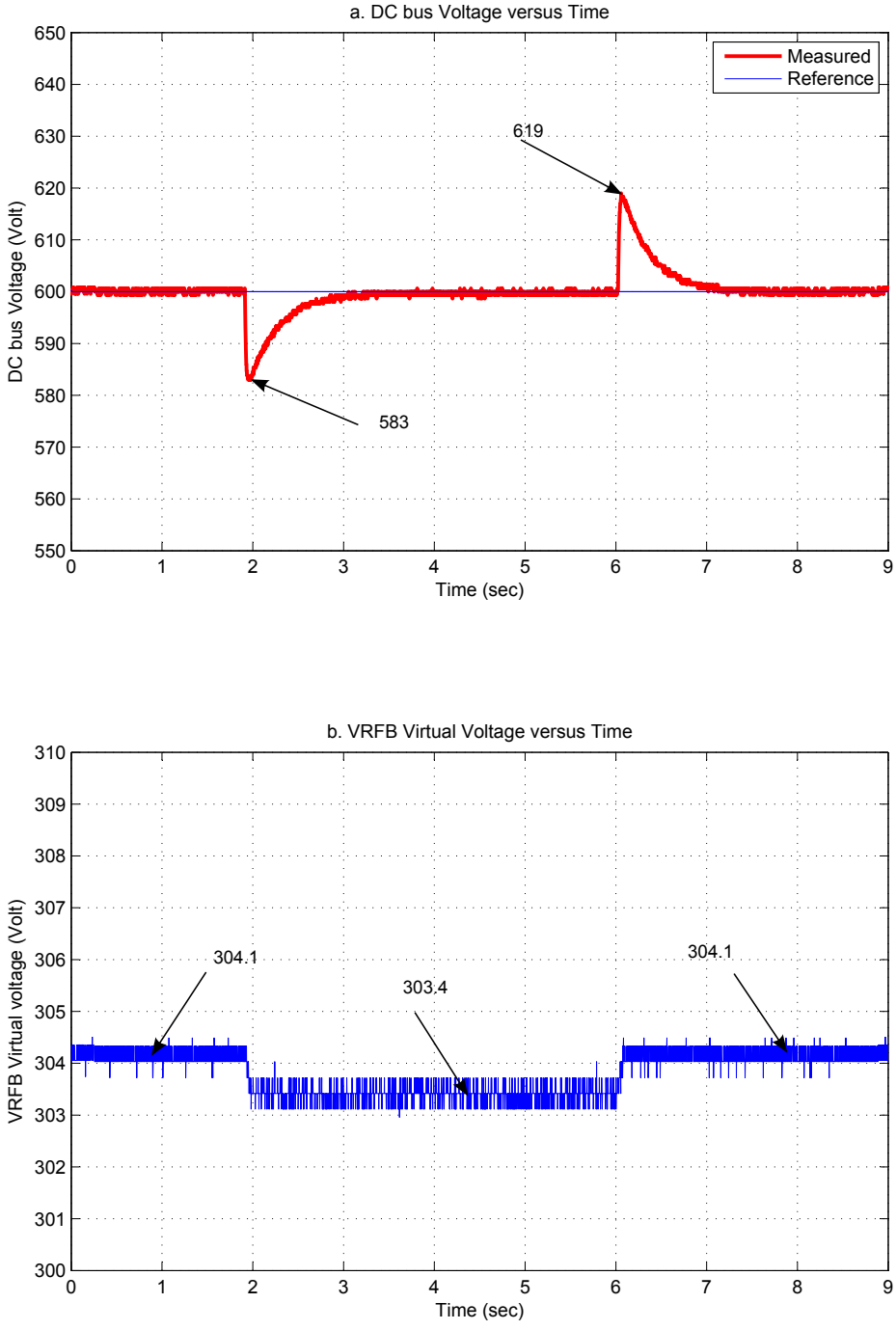

Figure 5-8: Experiments results without LI-IB: a. DC bus voltage. b. Virtual VRFB voltage.

5.3.2 VRFB and LI-IB

Case 1 : K = 1.0 and f_{lpf} = 10 Hz

Figures 5-9 and 5-10 are compared to Figures 5-3 and 5-4. The results of the experiments are equal to the results of the simulation.

Case 2 : K = 0.7 and f_{lpf} = 10 Hz

Figures 5-11, 5-12 are compared to Figures 5-5 and 5-6. The results of the experiments are equal to the results of the simulation.

From Tables 5.1, 5.2, 5.3 and 5.4, it validated the results from experiments with simulation results.

Case 3 : K = 0.5 and f_{lpf} = 10 Hz

It is shown in Figure 5-13 and Figure 5-14 , Table 5.3 and 5.4 that the DC bus voltage drop and over voltage is decreased compared to the previous cases due to drawing more current from the LI-IB during the transient when loads vary.

Case 4 : K = 0.3 and f_{lpf} = 10 Hz

It is shown in Figure 5-15 and Figure 5-16 , Table 5.3 and 5.4 that the DC bus voltage drop and over voltage is decreased more than the previous cases due to drawing more current from the LI-IB.

Case 4 : K = 0.3 and f_{lpf} = 5 Hz

It is shown in Figure 5-17 and Figure 5-18 , Table 5.3 and 5.4 that the DC bus voltage drop and over voltage is decreased more than the previous cases due to drawing more current from the LI-IB and the current will flow after the transient till reach to zero.

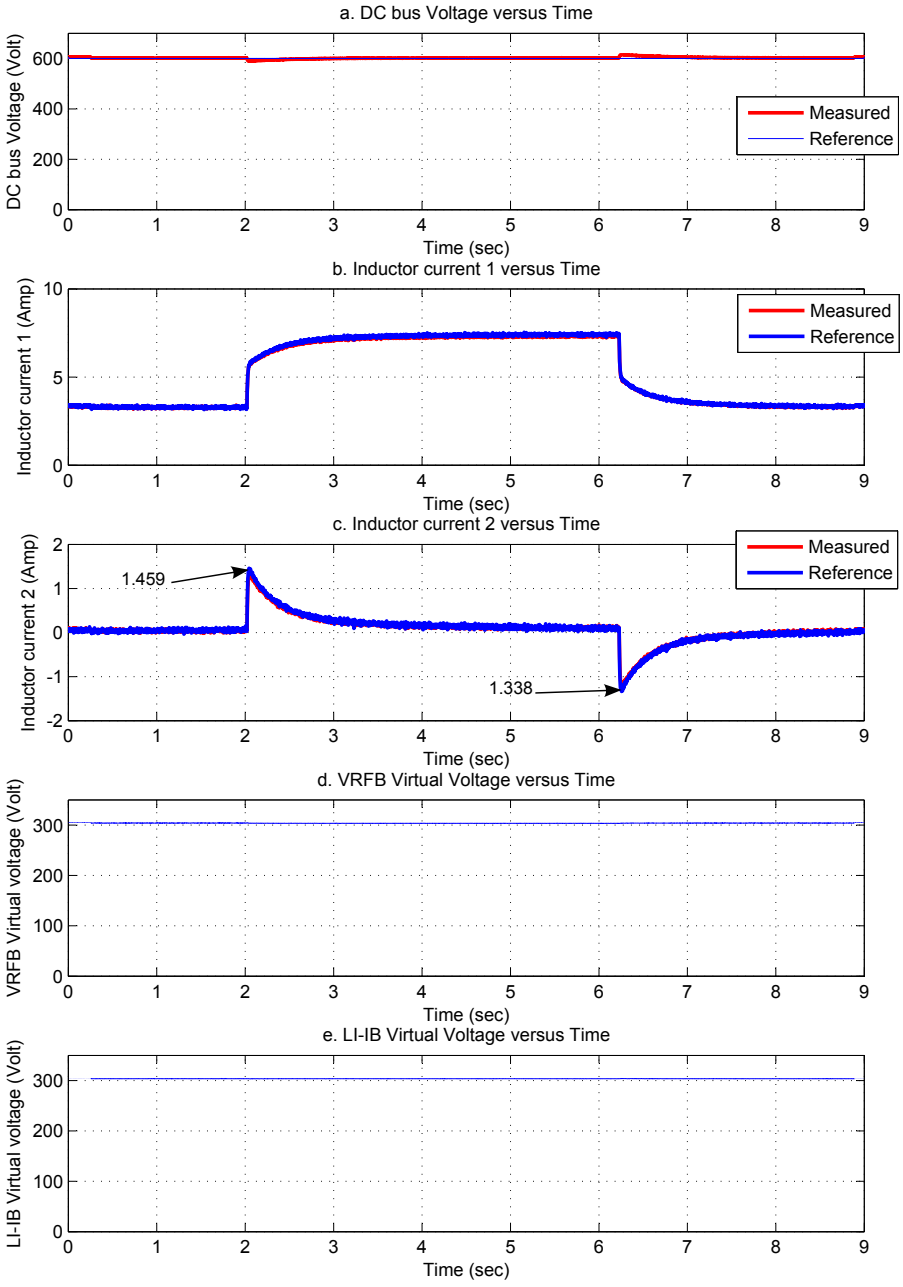

Figure 5-9: Experiments results at K = 1.0 and f_{lpf} = 10 Hz: a. DC bus voltage. b. VRFB current. c. LI-IB current. d. Virtual VRFB voltage. e. Virtual LI-IB voltage.

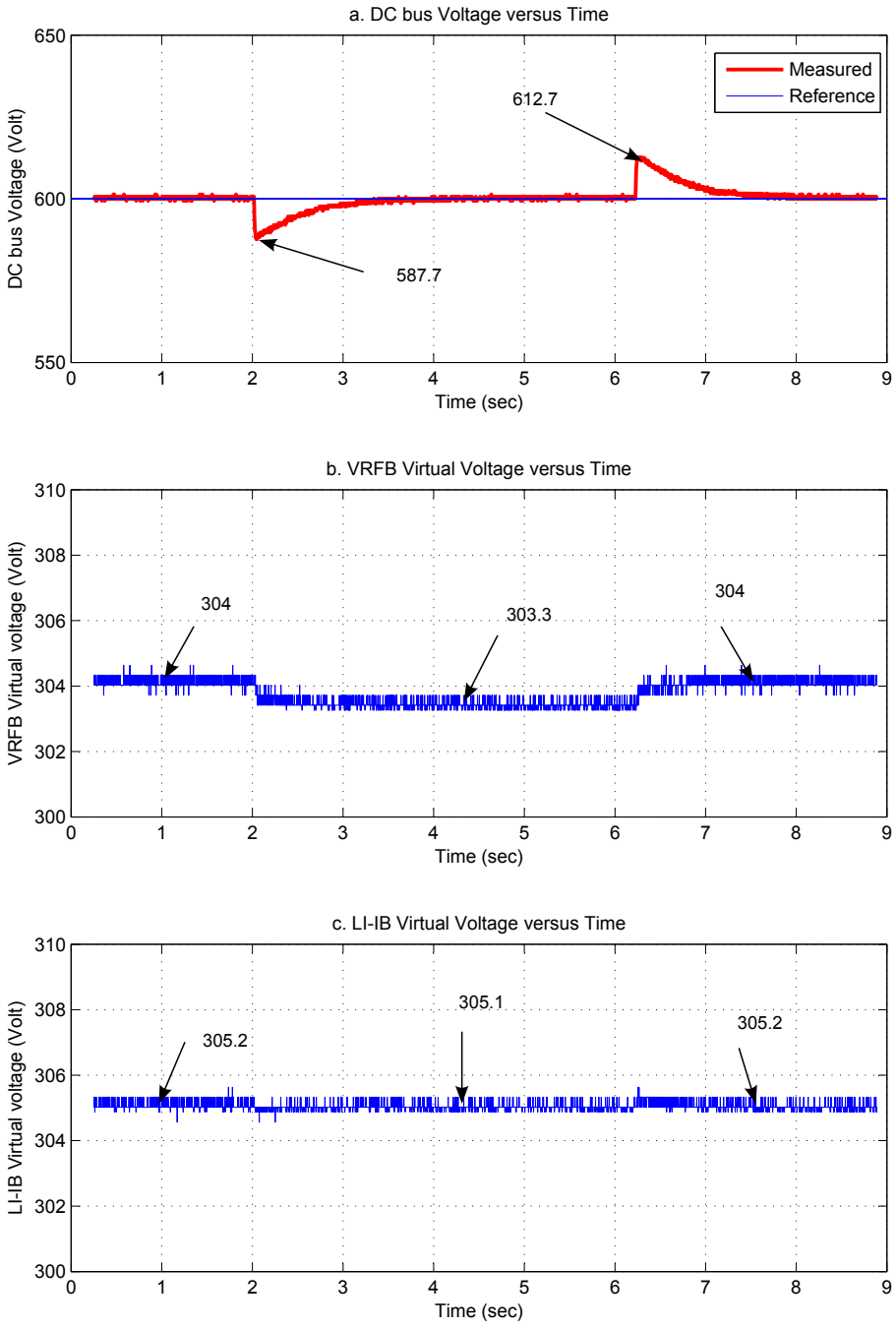

Figure 5-10: Experiments Results at K = 1.0 and f_{lpf} = 10 Hz: a. DC bus voltage. b. Virtual VRFB voltage. c. Virtual LI-IB voltage.

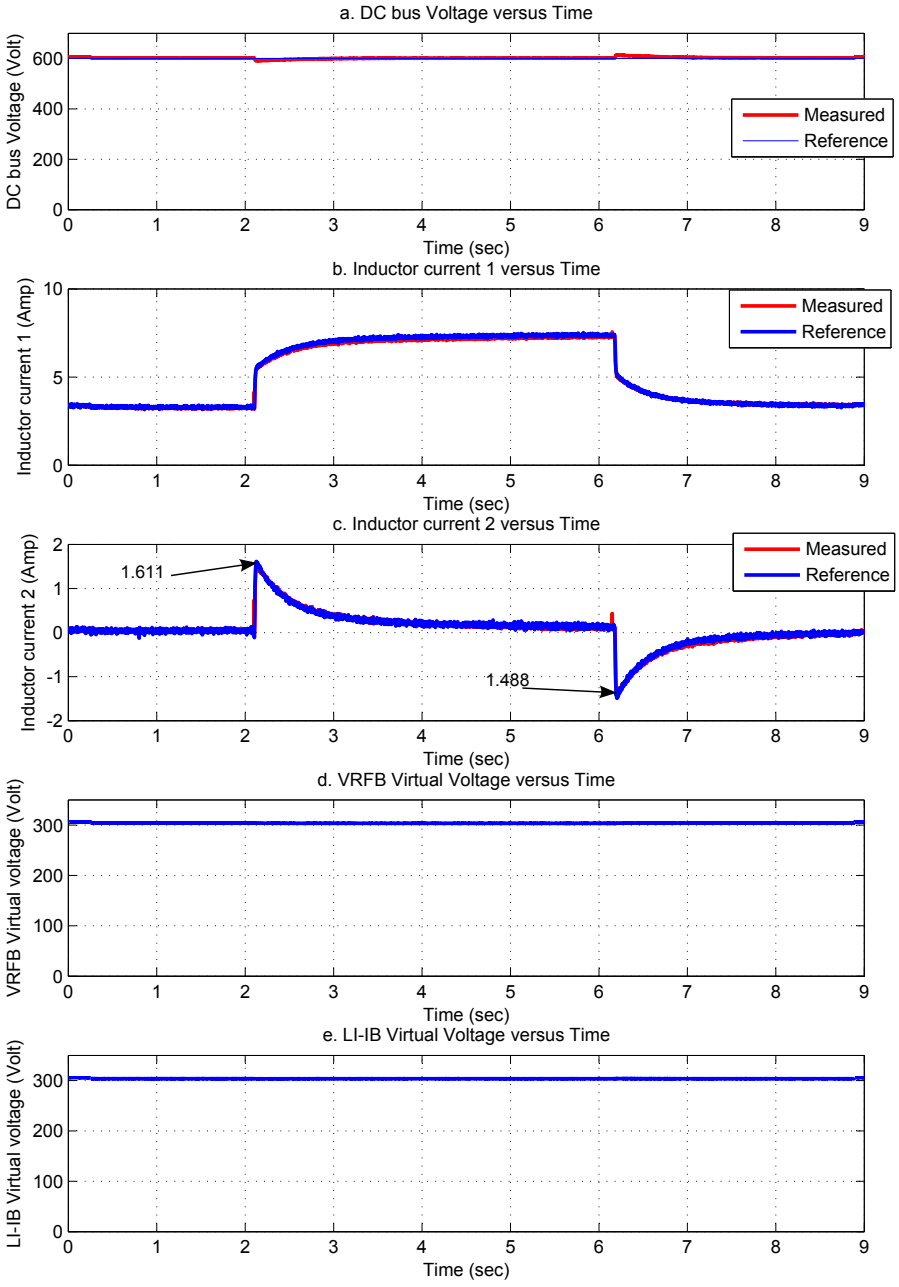

Figure 5-11: Experiments results at K = 0.7 and $f_{lpf} = 10$ Hz: a. DC bus voltage. b. VRFB current. c. LI-IB current. d. Virtual VRFB voltage. e. Virtual LI-IB voltage.

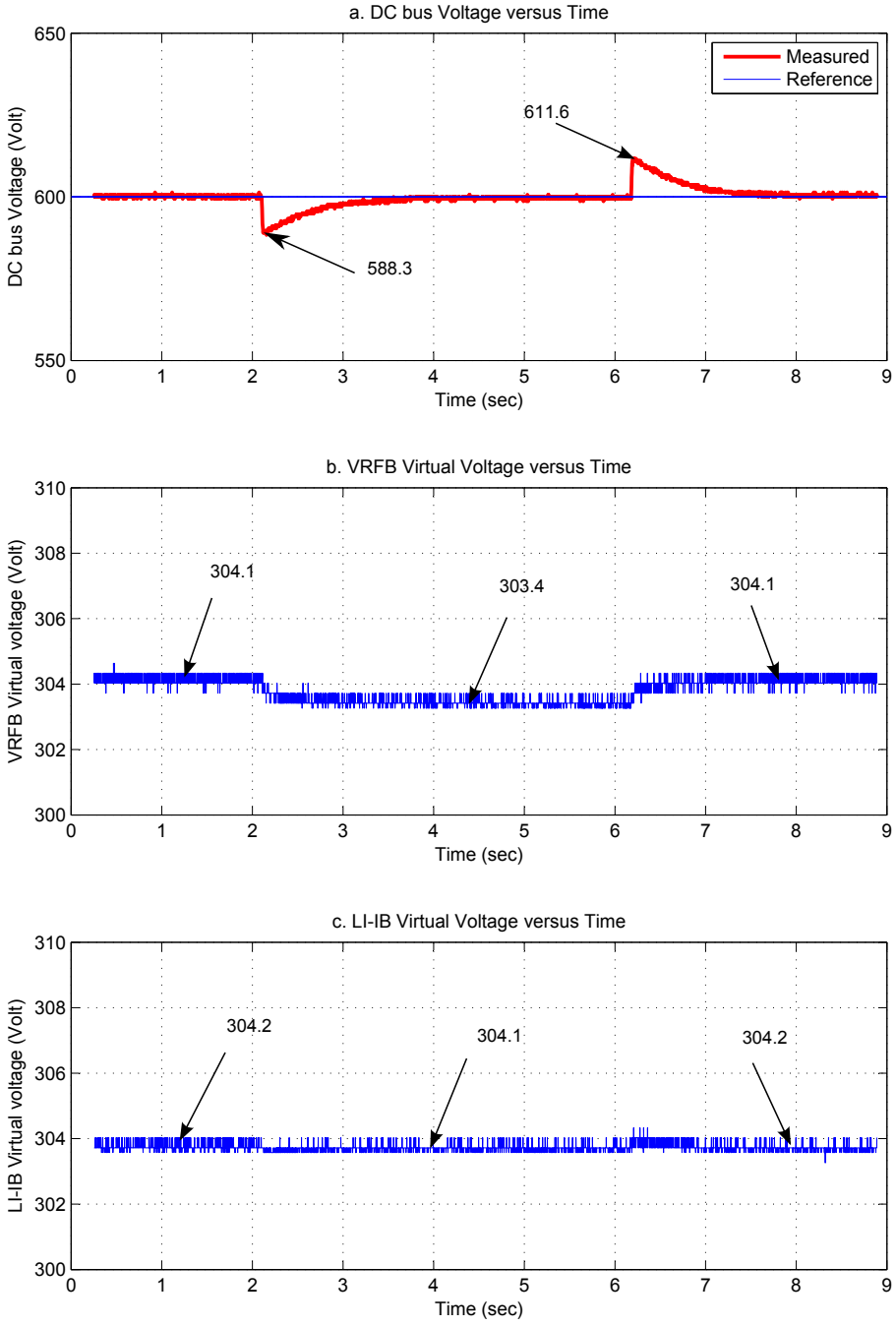

Figure 5-12: Experiments results at K = 0.7and $f_{lpf} = 10$ Hz: a. DC bus voltage. b. Virtual VRFB voltage. c. Virtual LI-IB voltage.

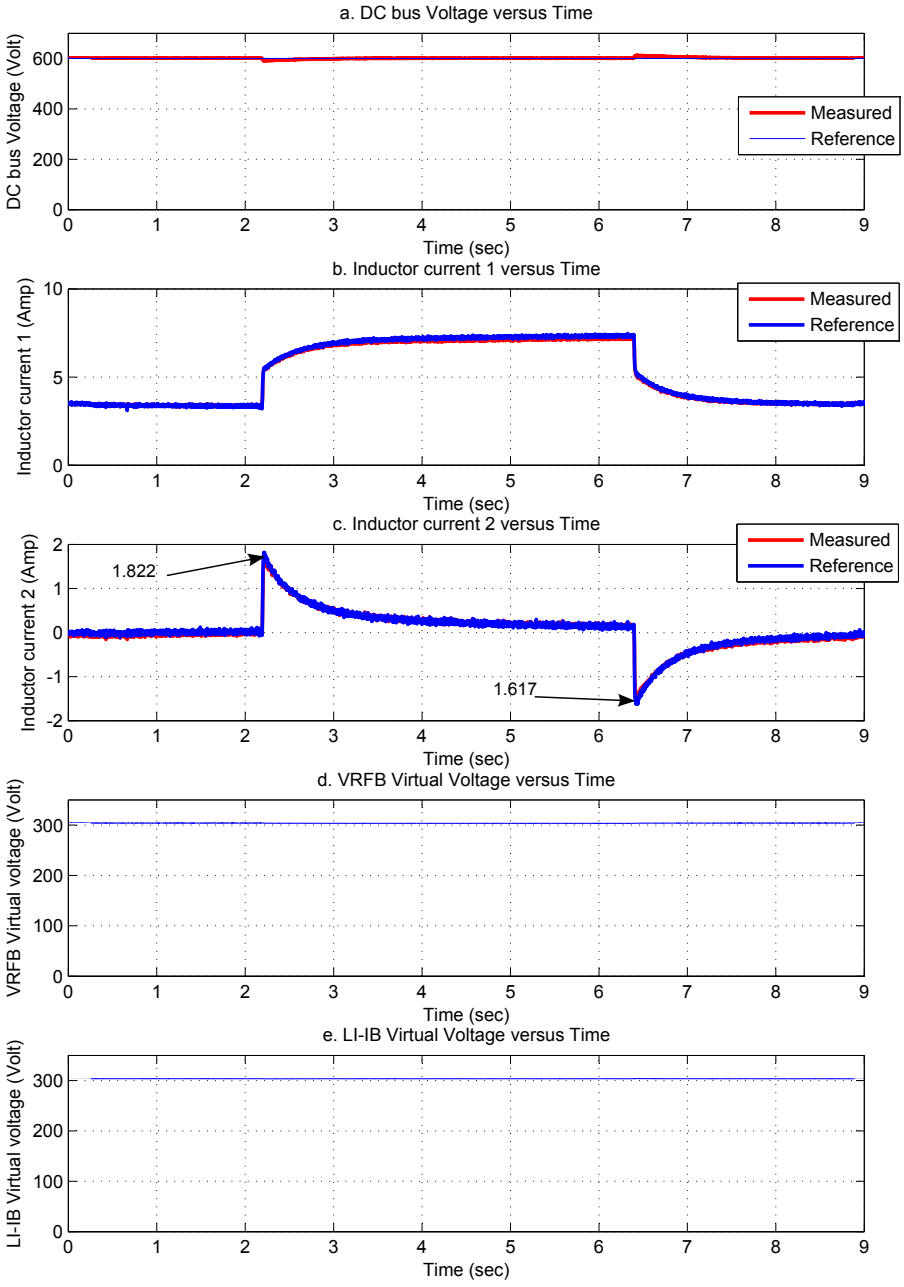

Figure 5-13: Experiments results at K = 0.5 and f_{lpf} = 10 Hz: a. DC bus voltage. b. VRFB current. c. LI-IB current. d. Virtual VRFB voltage. e. Virtual LI-IB voltage.

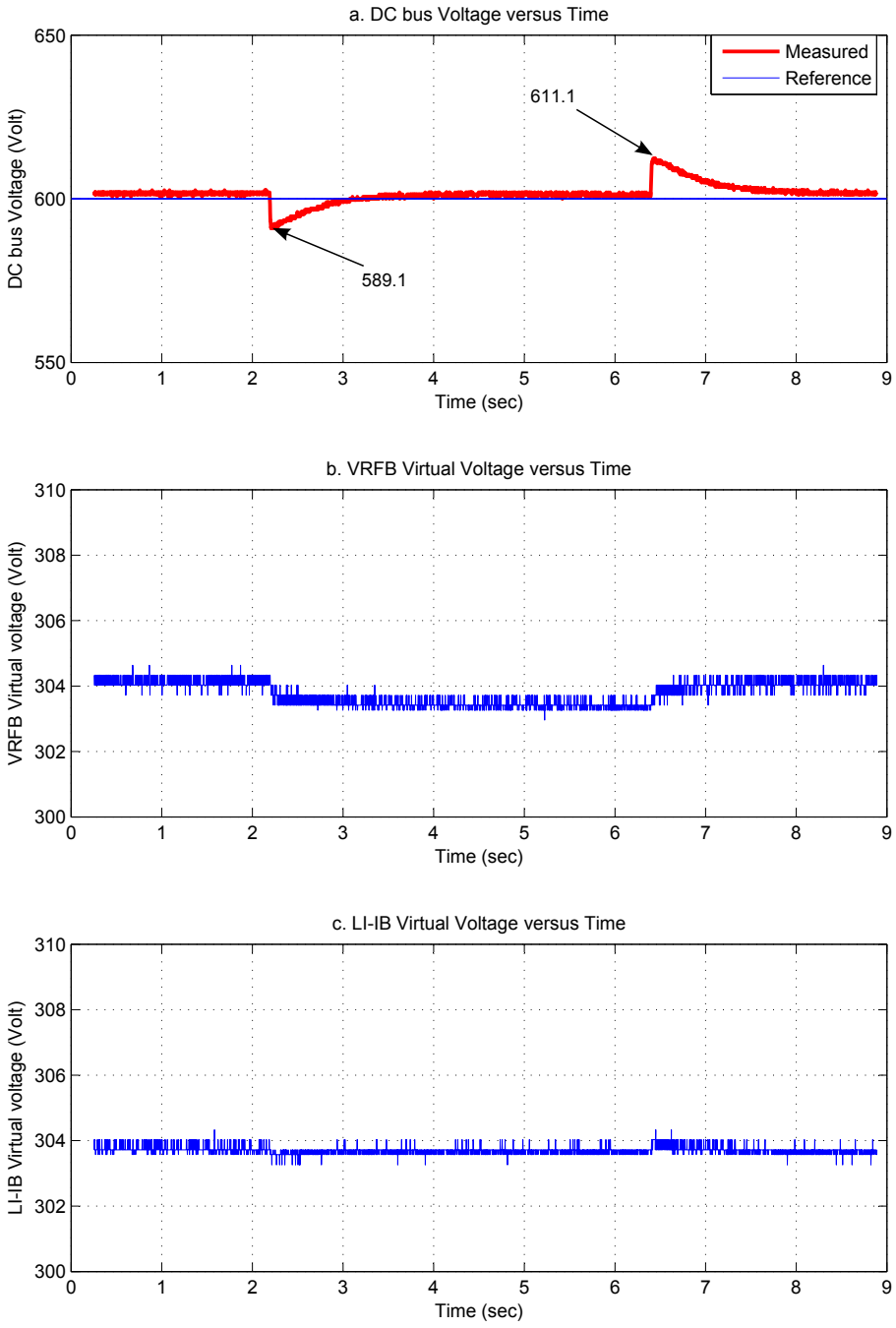

Figure 5-14: Experiments results at K = 0.5 and f_{lpf} = 10 Hz: a. DC bus voltage. b.Virtual VRFB voltage. c. Virtual LI-IB voltage.

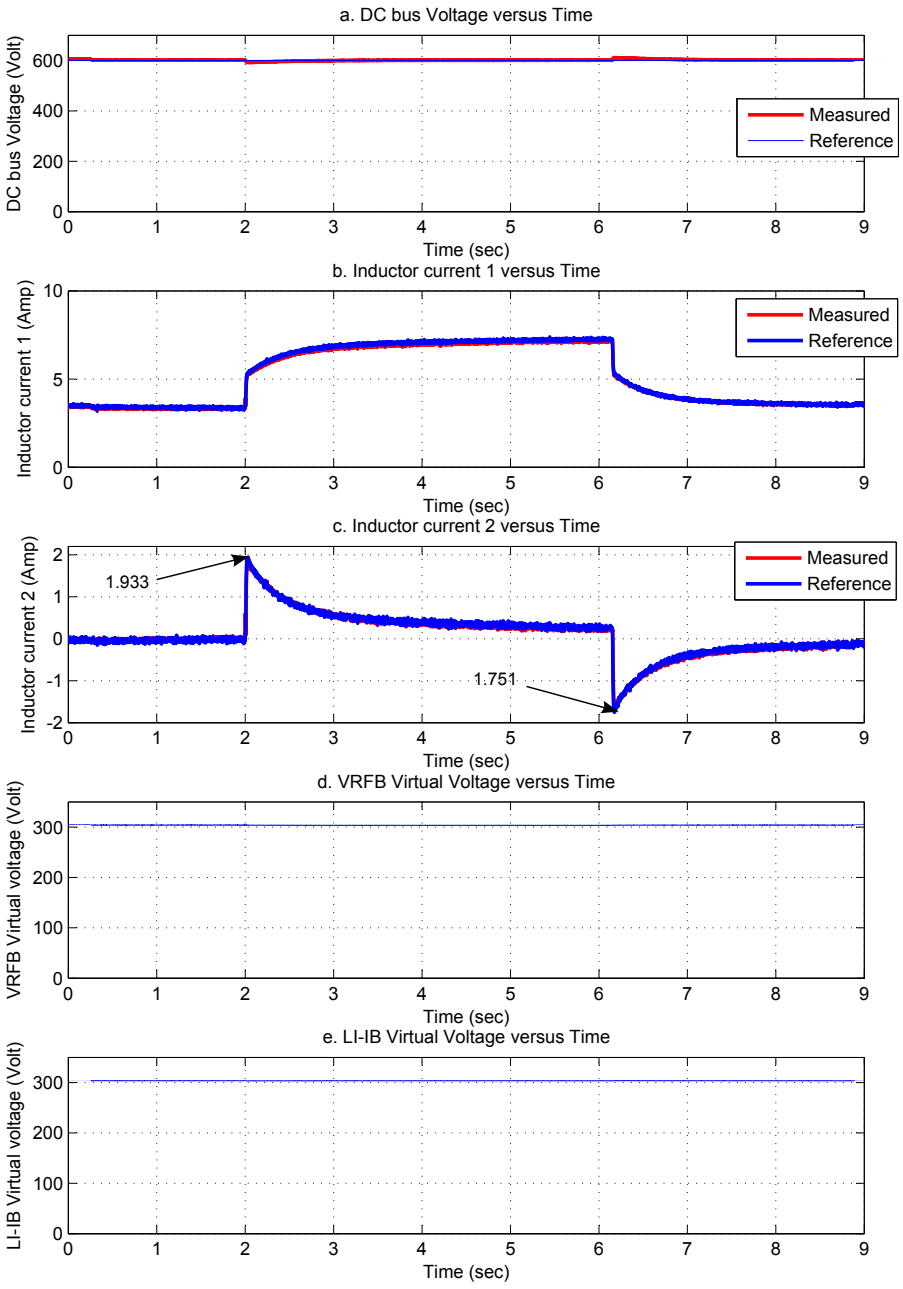

Figure 5-15: Experiments results at K = 0.3 and $f_{lpf} = 10$ Hz: a. DC bus voltage. b. VRFB current. c. LI-IB current. d. Virtual VRFB voltage. e. Virtual LI-IB voltage.

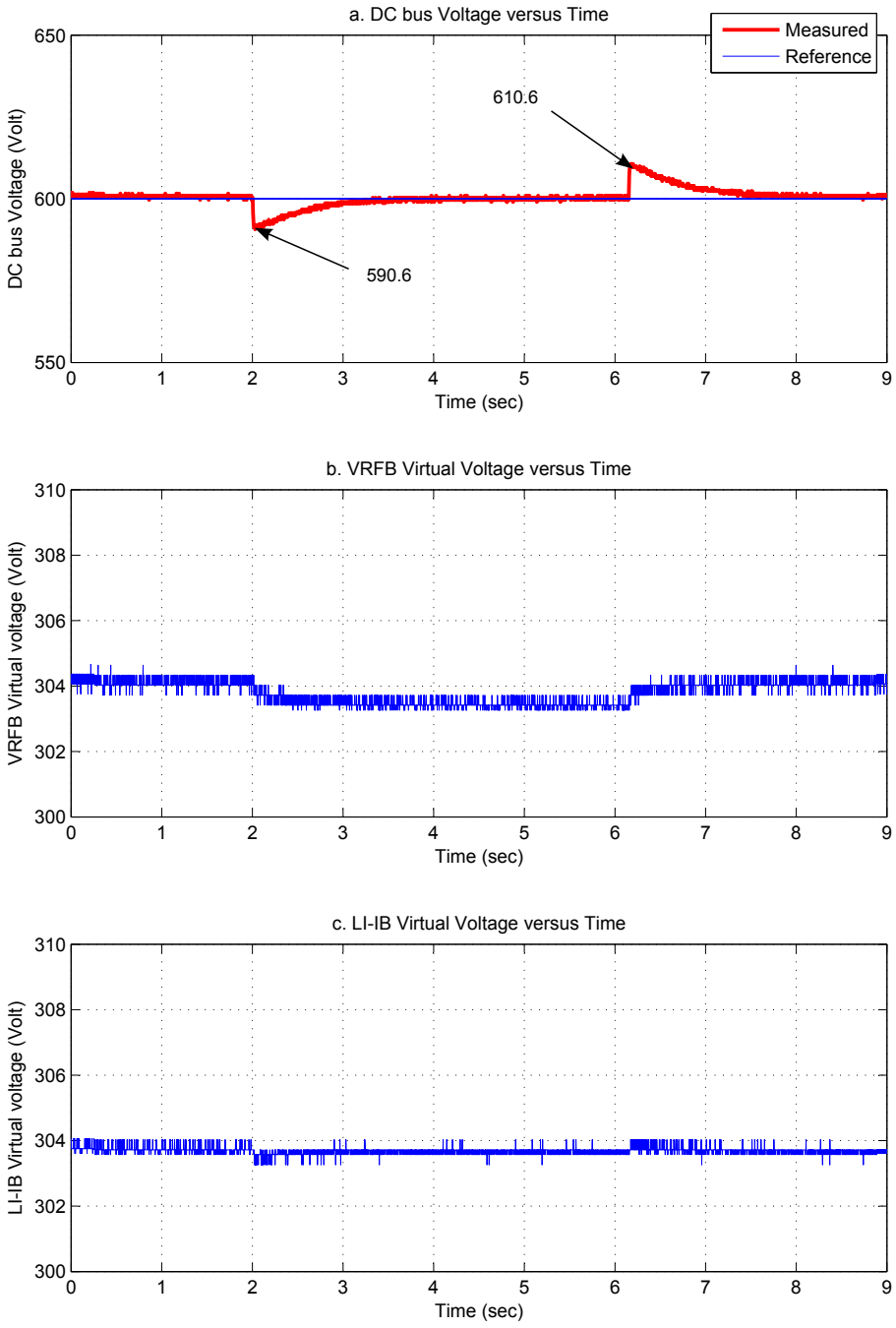

Figure 5-16: Experiments results at K = 0.3 and f_{lpf} = 10 Hz: a. DC bus voltage. b. Virtual VRFB voltage. c. Virtual LI-IB voltage.

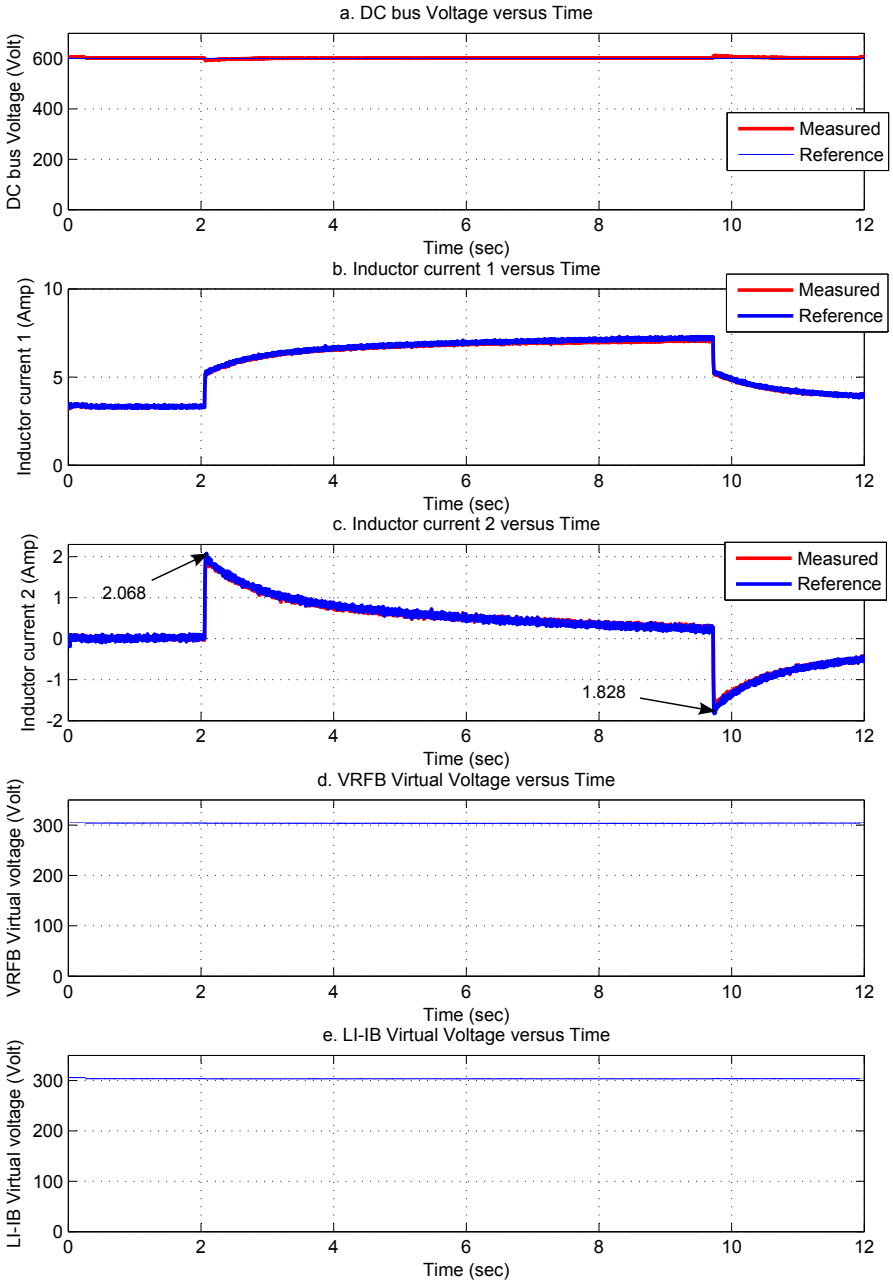

Figure 5-17: Experiments results at K = 0.3 and $f_{lpf} = 5$ Hz: a. DC bus Voltage. b. VRFB current. c. LI-IB current. d. Virtual VRFB voltage. e. Virtual LI-IB voltage.

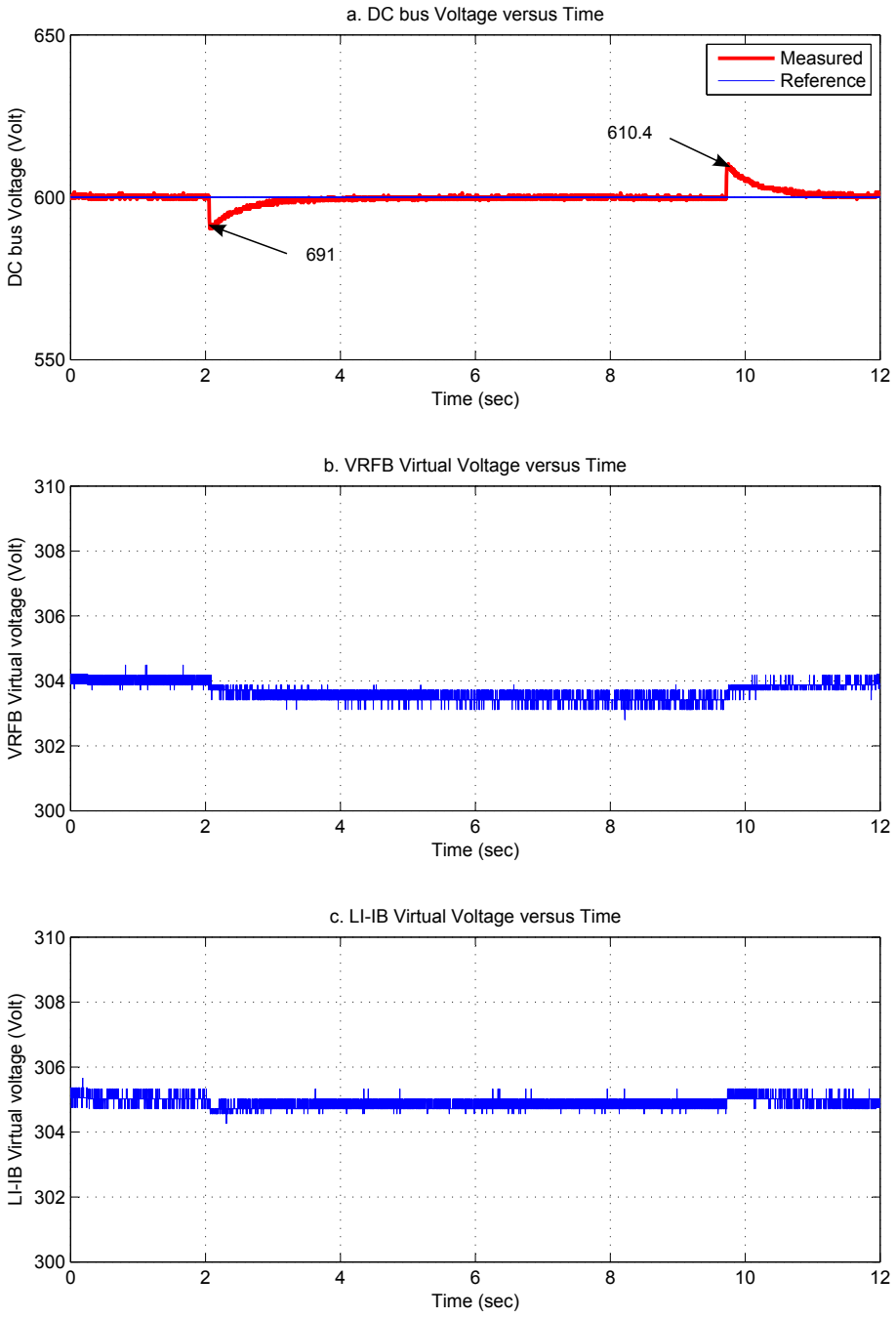

Figure 5-18: Experiments results at K = 0.3 and $f_{lpf} = 5$ Hz: a. DC bus Voltage. b. Virtual VRFB voltage. c. Virtual LI-IB voltage.

Table 5.3: DC Bus Voltage from Experiments Results

K	LPF frequency (Hz)	DC bus voltage when load 2 connected (Volt)	DC bus voltage load 2 disconnected (Volt)
Without LI-IB	Without LI-IB	583	619
1.0	10	587.7	612.7
0.7	10	588.3	611.6
0.5	10	589.1	611.1
0.3	10	590.6	610.6
0.3	5	591	610.4

Table 5.4: LI-IB Current from Experiments Results

k	LPF frequency (Hz)	LI-IB Current when load 2 connected (Amp)	LI-IB Current when load 2 disconnected (Amp)
1.0	10	1.459	1.388
0.7	10	1.611	1.488
0.5	10	1.822	1.617
0.3	10	1.933	1.751
0.3	5	2.068	1.828

Chapter 6

Conclusion and Future development

6.1 Conclusion

- Emulation of the batteries matches the simulation. A general model of VRFB has been implemented and is suitable for all power and energy ranges.

- The technique used for emulating of the batteries can be used for any technology of batteries, or even for another ESS (such as supercapacitors, regular capacitors, etc...). The behavior of any technique of batteries can be tested by using the same hardware. Only the changes will be in the software.

- The value of K in Figure 4-3 is changed from 1.0 to 0.3. A high decrease in the voltage drop and the over voltage of the DC bus at K = 0.3. This is because the current drawn from the LI-IB battery is increased when the controllable load 2 changed.

- The value of the frequency of the low pass filter in Figure 4-3 is changed from 10 Hz to 5 Hz. Also decrease in the voltage drop and the over voltage of the DC bus but in this case the current of the LI-IB will flow after the transient till reach to zero. Li-IB will supply the load for a while with VRFB.

- The Li-IB meets the real power need, by absorbing or delivering power as required by the system. By using HESS, it decreases the power range of the VRFB and consequently decreases the cost.
- The simulation results are validated with the experiments results from emulation the batteries.

6.2 Future development

- The results obtained from simulation and from experiments by emulating the batteries will be validated by testing real VRFB and LI-IB with the same power and energy ratings of both batteries.
- Optimization of bandwidth of controllers.
- Real-time parameters variation on the battery models.
- Hybridization of more than two ESS.
- Change the reference generation of the LI-IB current (e.g. considering load power instead of VRFB power, etc...). Optimization of the generation of the LI-IB current reference.
- DC bus voltage is controlled and the value of the DC bus voltage is changing depending on the battery capacity.
- A Three phase inverter will be connected to the DC bus from one side and the other side to the grid as shown in Figure 6-1. The control of the three phase inverter is to have the DC bus voltage constant around 600 volt. The control of the first bidirectional boost converter is power control to provide power in case the grid power is less than the load power and also to supply the loads in case of the interruption in the grid. The control of the second bidirectional boost converter is to supply the peak transient power when changing the loads and also in case of the interruption in the grid.

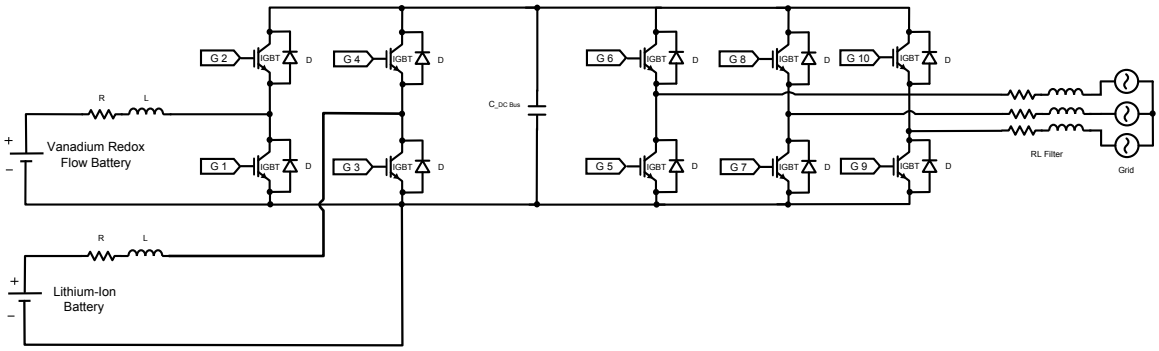

Figure 6-1: The power circuit of the system.

Appendix A

Figures

A.1 Experiments Results from the Oscilloscope

- Channel 1 is the DC bus voltage from the differential probe.
- Channel 2 is the VRFB current from the current probe.
- Channel 3 is the LI-IB current from the current probe.
- Channel 4 is the virtual voltage of the VRFB from the DSP.
- Channel 5 is the virtual voltage of the LI-IB from the DSP.
- Channel 6 is the reference current of the VRFB from the DSP.
- Channel 7 is the reference current of the LI-IB from the DSP.

A.2 Printed Circuit Boards (PCBs)

The boards are shown in Figures A-7, A-8, A-9, A-10 and A-11.

A.2.1 Three Phase Rectifier PCB

From the three phase rectifier board is used to get the initial value of the battery. There are two three phase rectifier boards for VRFB and LI-IB.

Figure A-1: Experiments results without LI-IB: a. DC bus voltage. b. VRFB current. c. Virtual VRFB voltage.

Figure A-2: Experiments results at K = 1.0 and f_{lpf} = 10 Hz: a. DC bus voltage. b. VRFB current. c. LI-IB current. d. Virtual VRFB voltage. e. Virtual LI-IB voltage.

Figure A-3: Experiments results at K = 0.7 and f_{lpf} = 10 Hz: a. DC bus voltage. b. VRFB current. c. LI-IB current. d. Virtual VRFB voltage. e. Virtual LI-IB voltage.

Figure A-4: Experiments results at K = 0.5 and f_{lpf} = 10 Hz: a. DC bus voltage. b. VRFB current. c. LI-IB current. d. Virtual VRFB voltage. e. Virtual LI-IB voltage.

Figure A-5: Experiments results at K = 0.3 and $f_{lpf} = 10$ Hz: a. DC bus Voltage. b. VRFB current. c. LI-IB current. d. Virtual VRFB voltage. e. Virtual LI-IB voltage.

Figure A-6: Experiments results at K = 0.3 and f_{lpf} = 5 Hz: a. DC bus Voltage. b. VRFB current. c. LI-IB current. d. Virtual VRFB voltage. e. Virtual LI-IB voltage.

A.2.2 Interface PCB

The interface board is adapting the sensors signals from GUASCH converter to the Filter and DSP board and also adapting the control signals from Filter and DSP board to the GUASCH converter.

A.2.3 Filter and DSP PCB

The Filter and DSP board is used to filter the sensors signals from GUASCH converter and also to control the GUASCH converter through the DSP.

A.2.4 USB PCB

The USB board is used to communicate between the DSP and the computer. This board s connected to the filter and DSP board.

A.2.5 Back Plane PCB

The back Plane board is used for the connect interface board with the filter and DSP board.

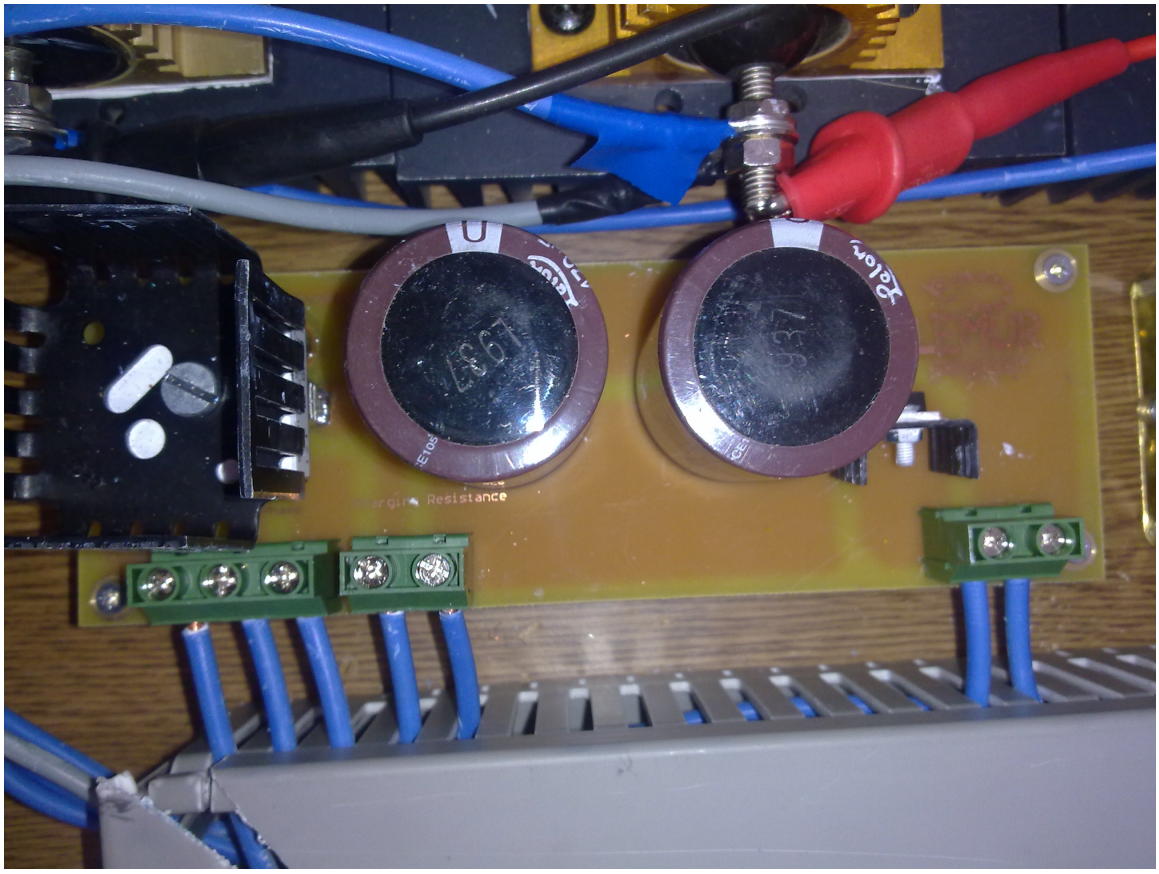

Figure A-7: Three phase rectifier board.

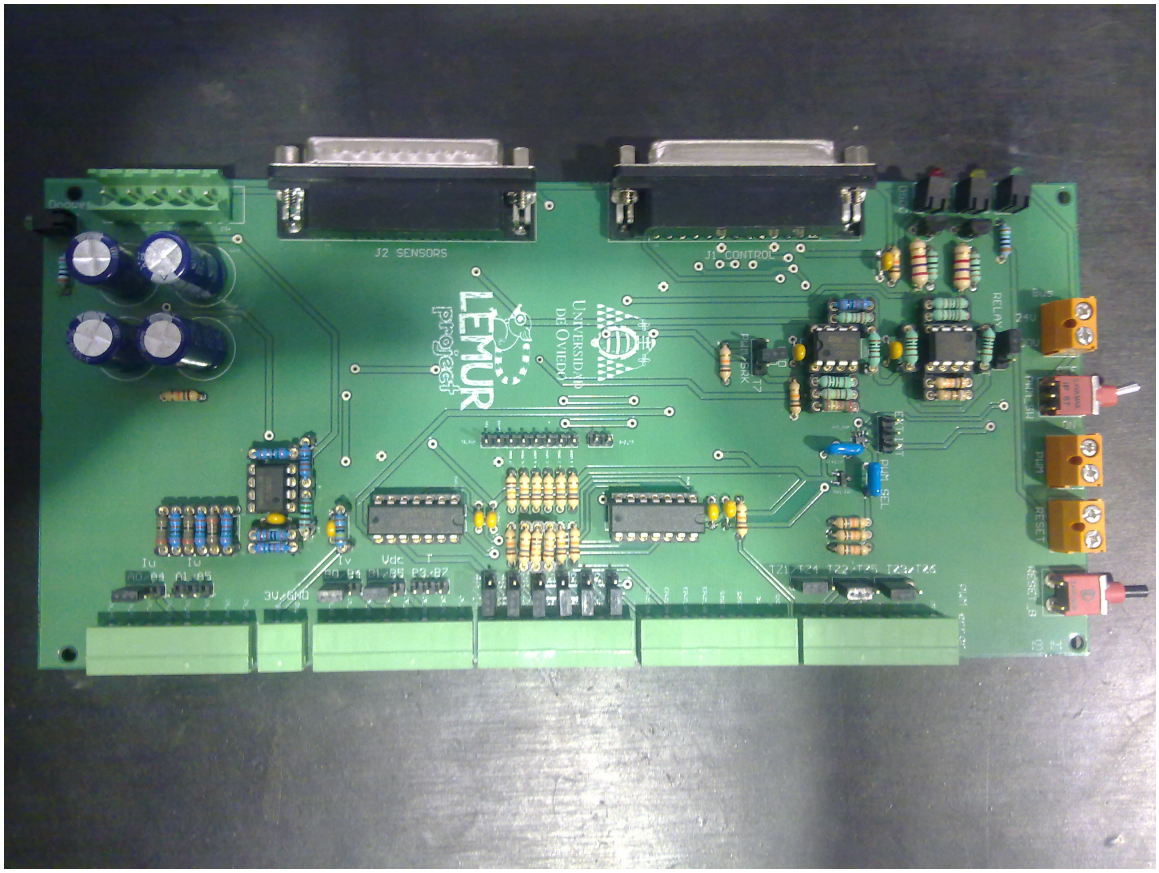

Figure A-8: Interface board.

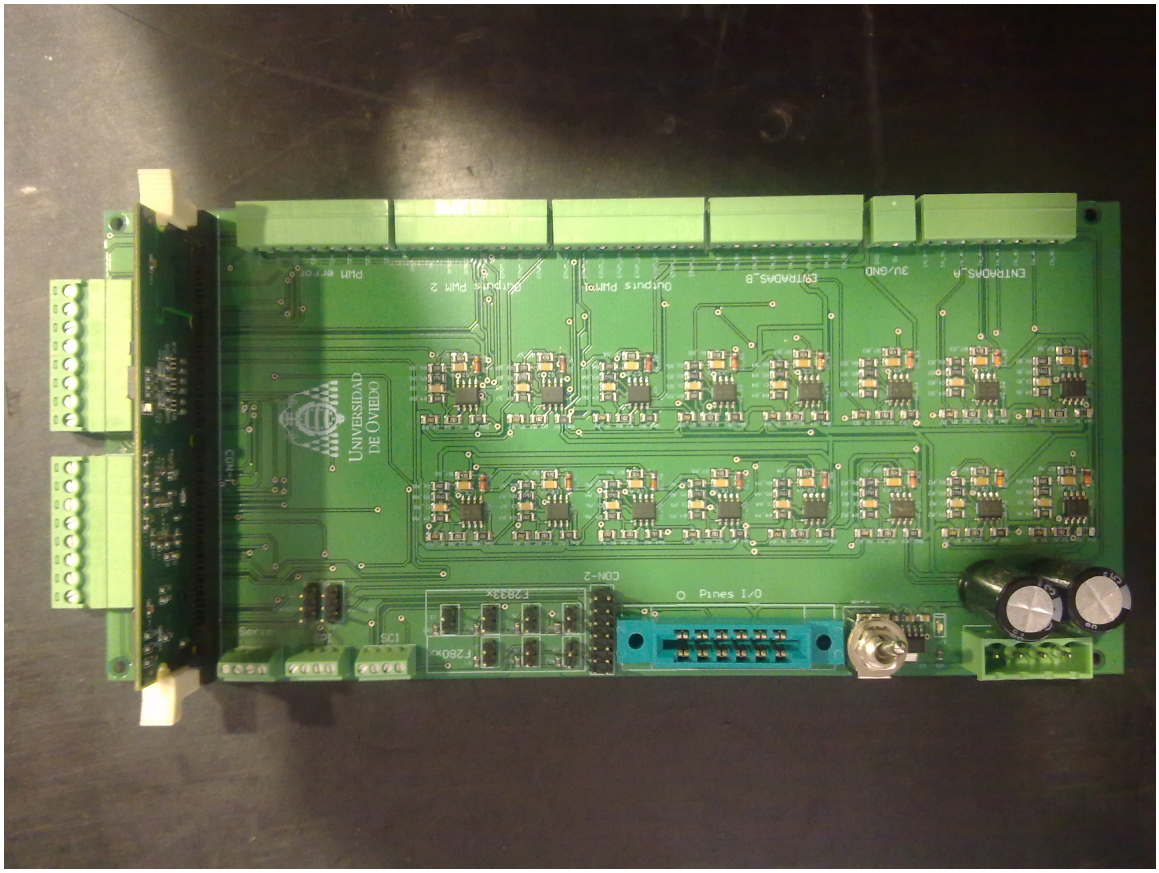

Figure A-9: Filter and DSP board.

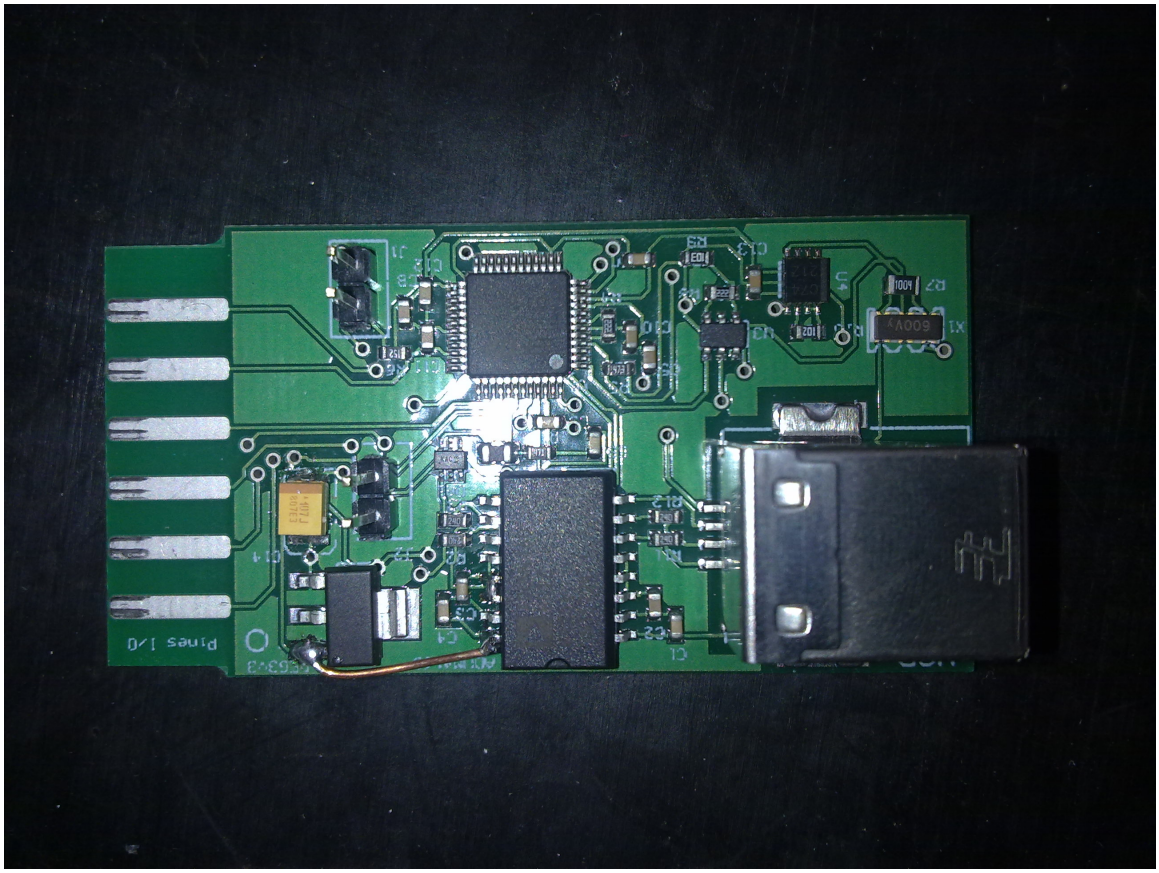

Figure A-10: USB board.

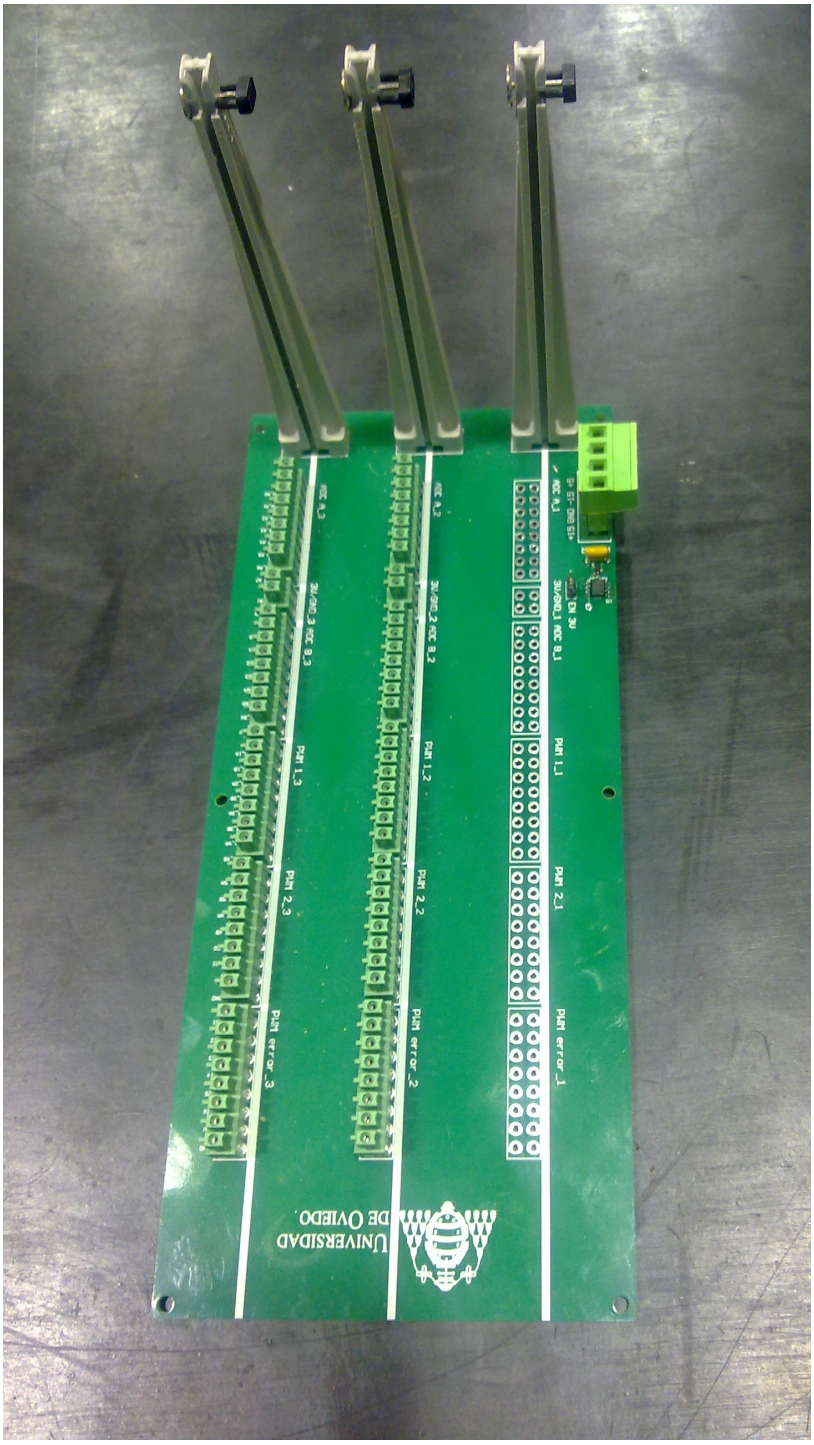

Figure A-11: Back plane board.

A.3 Experimental Setup

A.3.1 Manual Control

The manual control is used to supply the power to the boards. It also used to connect or disconnect the Loads from the two boost converter. It is shown in Figure A-12.

A.3.2 Inductors

The inductors are used for first and second boost converter are shown in Figure A-13.

A.3.3 GUASCH Converter

The GUASCH converter in Figure A-14 is used to implement two bidirectional boost converter. It has a DC bus , voltage sensor of the DC bus and two current sensors for the inductors current.

A.3.4 Total Setup

Figure A-15 shows the total setup of the hardware.

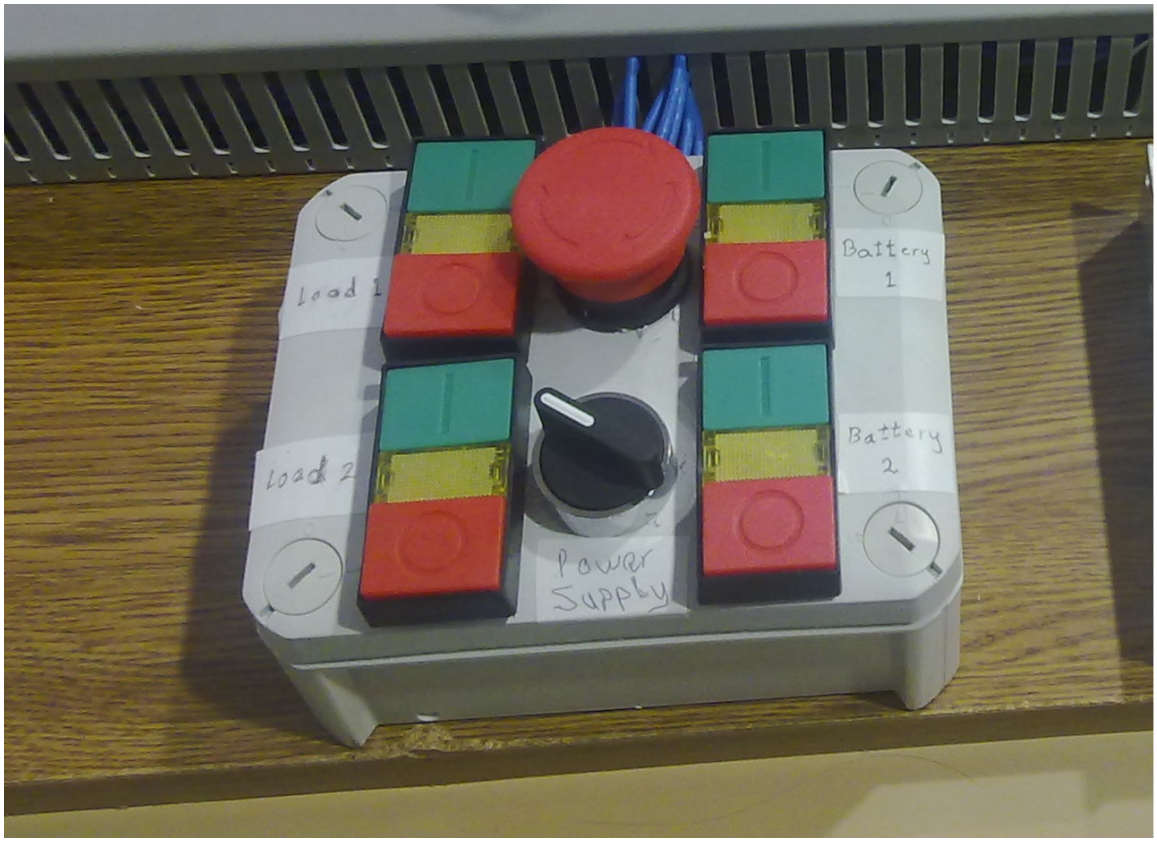

Figure A-12: Manual Control.

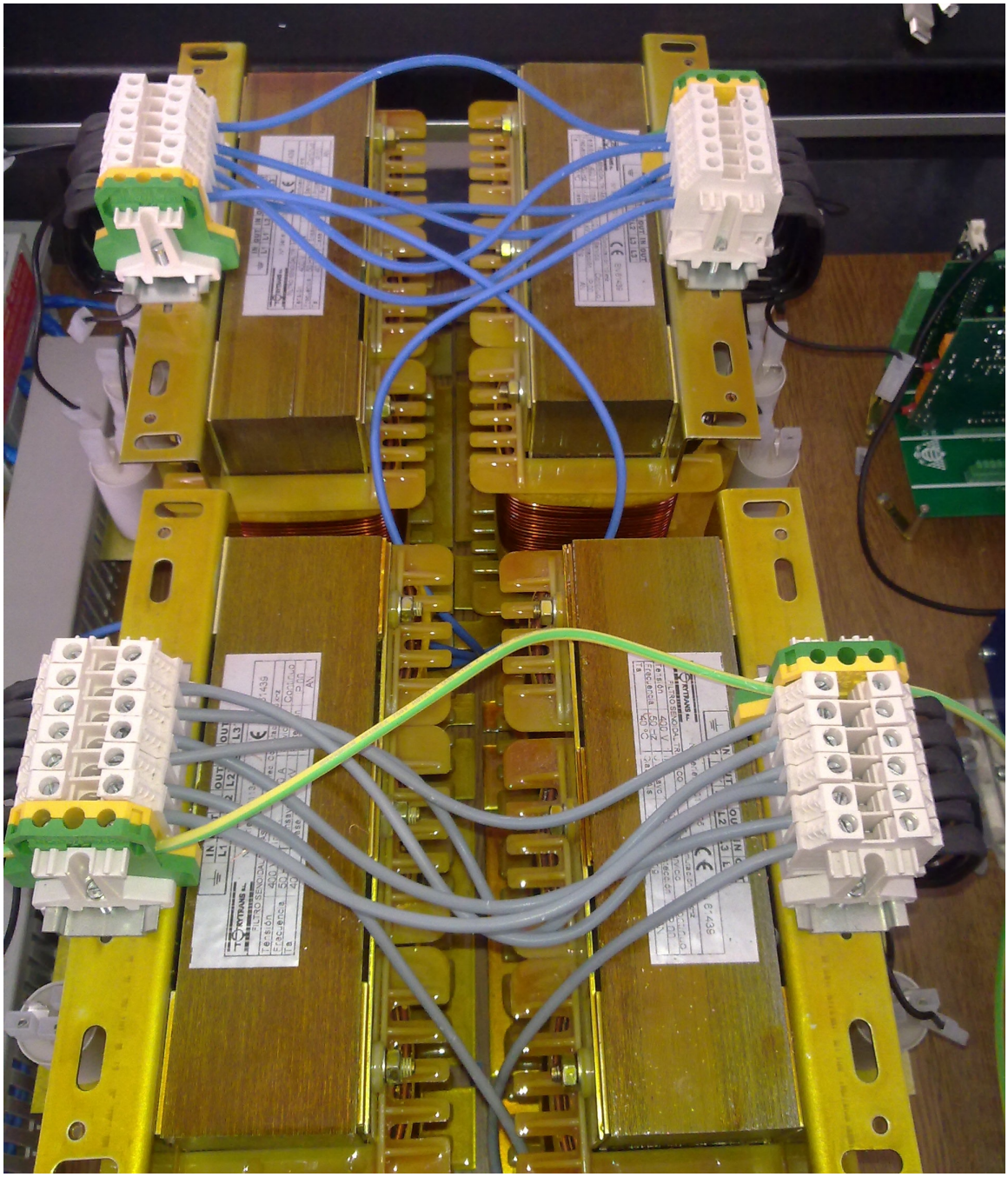

Figure A-13: Inductors of the first and second boost converters.

Figure A-14: GUASCH Converter.

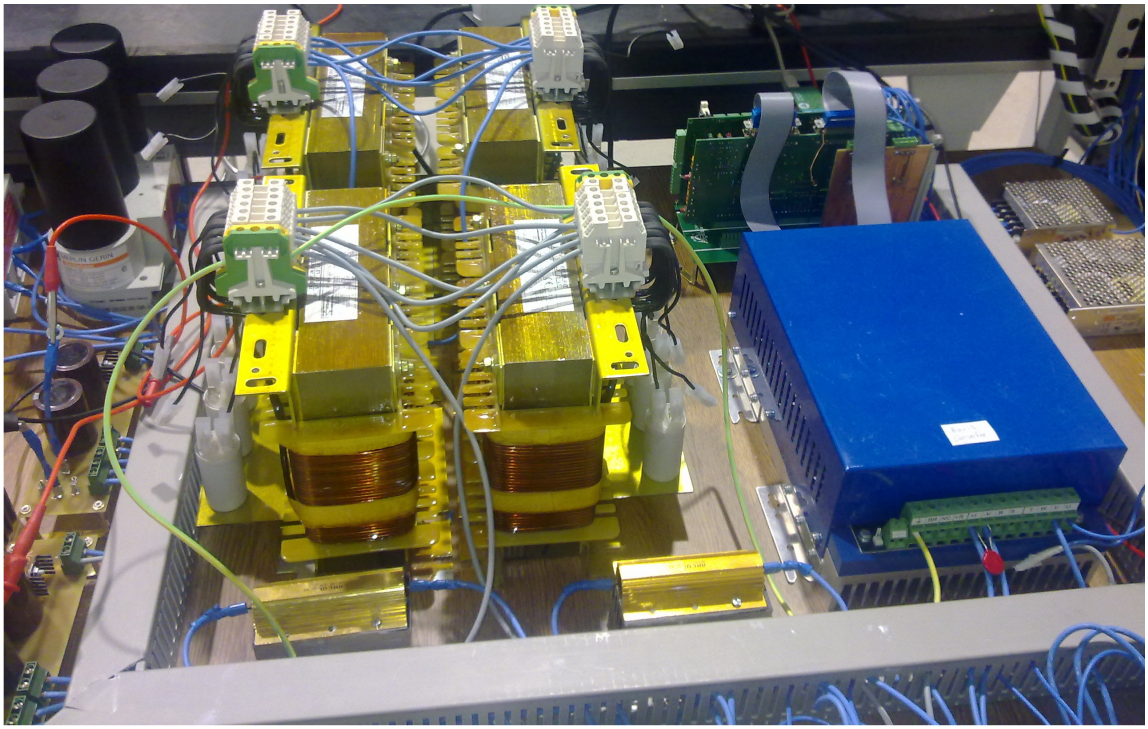

Figure A-15: Total setup.

Bibliography

[1] H. Camblong I. Vechiu, A. Etxeberria and J. M. Vinassa, "Advanced power electronic interface for hybrid energy storage system used for microgrids".

[2] H. Camblong I. Vechiu, A. Etxeberria and J. M. Vinassa, "Three-level neutral point clamped inverter interface for flow battery/supercapacitor energy storage system used for microgrids", In *IEEE*.

[3] Sowmini priya.S and Rajakumar.S, "An energy storage system for wind turbine generators- battery and supercapacitor", *International Journal of Engineering Research and Applications (IJERA)*, 3:1219 – 1223, March - April 2013.

[4] Baohui Zhang Bo Wang and Zhiguo Hao, "Control of composite energy storage system in wind and pv hybrid microgrid", In *IEEE*, 2013.

[5] Haihua Zhou Duong Tran and Ashwin M. Khambadkone, "Energy management and dynamic control in composite energy storage system for micro-grid applications", In *IEEE*, pages 1818 – 1824, 2010.

[6] H. Camblong A. Etxeberria J.M. Vinassa A. Etxeberria, I. Vechiu and H. Camblong, "Hybrid energy storage systems for renewable energy sources integration in microgrids: A review", In *IEEE IPEC*, pages 532 – 537, 2010.

[7] John A. Chahwan, "Vanadium-Redox Flow and lithium-ion battery modelling and performance in wind energy applications", Master's thesis, McGill University, Montreal, Quebec, May 2007.

[8] C. Marinescu L. Barote and M. Georgescu, "VRB modeling for storage in stand-alone wind energy systems", In *IEEE Bucharest Power Tech Conference*, Bucharest, Romania, June 2009.

[9] Ye Zhang Li Guo and Cheng Shan Wang, "A new battery energy storage system control method based on soc and variable filter time constant", In *IEEE*, 2011.

[10] Jordi Pegueroles-Queralt Fernando A. Inthamoussou and Fernando D. Bianchi, "Control of a supercapacitor energy storage system for microgrid applications", *IEEE TRANSACTIONS ON ENERGY CONVERSION*, 28(3):690 – 697, September 2013.

[11] C. A. Smith D. D. Banham-Hall, G. A. Taylor and M. R. Irving, "Frequency control using vanadium redox flow batteries on wind farms", In *IEEE*, 2011.

[12] C. Abbey J. Chahwan and G. Joos, "VRB modelling for the study of output terminal voltages, internal losses and performance", In *IEEE Canada Electrical Power Conference*, 2007.

[13] Wei Li and Geza Joos, "A power electronic interface for a battery supercapacitor hybrid energy storage system for wind applications", In *IEEE*, pages 1762 – 1768, 2008.

[14] Wu Bingyin Mao Biao, Zhang Buhan and Xie Guanglong, "Studies on security capacity of wind farms containing vrb energy storage system", In *Mao Biao*, pages 1704 – 1708.

[15] Daqiang Bi Wenliang Wang, Baoming Ge and Dongsen Sun, "Grid-connected wind farm power control using vrb-based energy storage system", In *IEEE*, pages 3772 – 3777, 2010.

[16] Geza Joos Wei Li and Jean Belanger, "Real-time simulation of a wind turbine generator coupled with a battery supercapacitor energy storage system", *IEEE TRANSACTIONS ON INDUSTRIAL ELECTRONICS*, 57(4):1137 – 1145, April 2010.

[17] D.Faiman M. Averbukh and K.Batat, "Modeling of dynamic behavior of vanadium redox batteries (vrb) with contamination properties of proton exchange membrane", In *IEEE 27th Convention of Electrical and Electronics Engineers*, Israel, 2012.

[18] Christian Blanc, "Modeling of a Vanadium Redox Flow Battery Electricity Storage System", PhD thesis, ECOLE POLYTECHNIQUE FEDERALE DE LAUSANNE, 24 April 2009.

[19] Thoshitha T. Gamage M. L. Crow Bruce M. McMillin Tu A. Nguyen, Xin Qiu and A. C. Elmorey, "Microgrid application with computer models and power management integrated using pscad/emtdc".

[20] Ming Ding Zhong Chen and Jianhui Su, "Modeling and control for large capacity battery energy storage system", pages 1429 – 1436.

[21] M. L. Crow A. C. Elmore Xin Qiu, Tu Nguyen and B. McMillin, "Computer models for microgrid applications", In *IEEE*, 2011.

[22] Martin Harrer Martha Schreiber, Adam H. Whitehead and Rene Moser, "The vanadium redox battery - an energy reservoir for stand-alone its applications along motor- and expressways", In *IEEE Conference on Intelligent Transportation Systems*, pages 936 – 940, Vienna, Austria, 13-16 September 2005.

[23] R. Teodorescu C. Marinescu L. Barote, R. Weissbach and M. Cirstea, "Stand-alone wind system with vanadium redox battery energy storage",

[24] L. Barote and C. Marinescu, "A new control method for vrb soc estimation in stand-alone wind energy systems", In *IEEE*, pages 253 – 257, 2009.

[25] J. M. Hawkins and T.P. Robbins, "A field trial of a vanadium energy storage system", In *INTELEC, lEE*, number 484, pages 652 – 656, 14-18 October 2001.

[26] Chris A. Smith Dominic D. Banham-Hall, Gareth A. Taylor and Malcolm R. Irving, "Flow batteries for enhancingwind power integration", *IEEE TRANSACTIONS ON POWER SYSTEMS*, 27(3):1690 – 1697, August 2012.

[27] M. Gonzaleza V.M. Garciab C. Blancoa D. Anseana, J.C. Vieraa and J.L. Antunaa, "Meaurement and study of dc internal resistance in lifepo4 batteries", In *EEVC European Electric Vehicle Congress*, Brussels, Belgium, November 2012.

[28] Zhuo Fang Liu Baoquan and Bao Xianwen, "Control method of the transient compensation process of a hybrid energy storage system based on battery and ultra-capacitor in micro-grid", In *IEEE*, pages 1325 – 1329, 2012.

[29] Toshifumi Ise Hiroaki Kakigano, Yushi Miura and Ryohei Uchida, "Dc micro-grid for super high quality distribution - system configuration and control of distributed generations and energy storage devices -".

[30] Jun Liang and Chunmei Feng, "Stability improvement of micro-grids with coordinate control of fuel cell and ultracapacitor", In *IEEE*, pages 2472 – 2477, 2007.

[31] Toshiaki Murata Junji Tamura Masahiro Kubo Akira Kuwayama Tomoki Asao, Rion Takahashi and Takatoshi Matsumoto, "Smoothing control of wind power generator output by superconducting magnetic energy storage system", In *Proceeding of International Conference on Electrical Machines and Systems*, pages 302 – 307, Seoul, Korea, October 2007.

[32] Xiwang Cui Yong Li Xiaojuan Han, Fang Chen and Xiangjun Li, "A power smoothing control strategy and optimized allocation of battery capacity based on hybrid storage energy technology", *Energies*, 5:1593–1612, May 2012.

[33] Gentaro Koshimizu Katsuhisa Yoshimoto, Toshiya. Nanahara and Yoshihsa Uchida, "New control method for regulating state-of-charge of a battery in hybrid wind power/battery energy storage system", In *IEEE PSCE*, pages 1244 – 1251, 2006.